

MIT Open Access Articles

Reprogramming of tRNA modifications controls the oxidative stress response by codon-biased translation of proteins

The MIT Faculty has made this article openly available. **Please share** how this access benefits you. Your story matters.

Citation: Chan, Clement T.Y. et al. "Reprogramming of tRNA Modifications Controls the Oxidative Stress Response by Codon-biased Translation of Proteins." Nature Communications 3 (2012): 937.

As Published: <http://dx.doi.org/10.1038/ncomms1938>

Publisher: Nature Publishing Group

Persistent URL: <http://hdl.handle.net/1721.1/76775>

Version: Author's final manuscript: final author's manuscript post peer review, without publisher's formatting or copy editing

Terms of Use: Article is made available in accordance with the publisher's policy and may be subject to US copyright law. Please refer to the publisher's site for terms of use.



Reprogramming of tRNA modifications controls the oxidative stress response by codon-biased translation of proteins

Clement T.Y. Chan,^{1,2} Yan Ling Joy Pang,¹ Wenjun Deng,¹ I. Ramesh Babu,¹ Madhu Dyavaiah,³ Thomas J. Begley³ and Peter C. Dedon^{1,4*}

¹Department of Biological Engineering, ²Department of Chemistry and ⁴Center for Environmental Health Sciences, Massachusetts Institute of Technology, Cambridge, MA 02139; ³College of Nanoscale Science and Engineering, University at Albany, SUNY, Albany, NY 12203

* Corresponding author: PCD, Department of Biological Engineering, NE47-277, Massachusetts Institute of Technology, 77 Massachusetts Avenue, Cambridge, MA 02139; tel 617-253-8017; fax 617-324-7554; email pcdedon@mit.edu

ABSTRACT

Selective translation of survival proteins is an important facet of cellular stress response. We recently demonstrated that this translational control involves a stress-specific reprogramming of modified ribonucleosides in tRNA. Here we report the discovery of a step-wise translational control mechanism responsible for survival following oxidative stress. In yeast exposed to hydrogen peroxide, there is a Trm4 methyltransferase-dependent increase in the proportion of tRNA^{LEU(CAA)} containing m⁵C at the wobble position, which causes selective translation of mRNA from genes enriched in the TTG codon. Of these genes, oxidative stress increases protein expression from the TTG-enriched ribosomal protein gene *RPL22A*, but not its unenriched paralog. Loss of either *TRM4* or *RPL22A* confers hypersensitivity to oxidative stress. Proteomic analysis reveals that oxidative stress causes a significant translational bias toward proteins coded by TTG-enriched genes. These results point to stress-induced reprogramming of tRNA modifications and consequential reprogramming of ribosomes in translational control of cell survival.

INTRODUCTION

Decades of study have revealed more than 100 ribonucleoside structures incorporated as post-transcriptional modifications mainly in tRNA and rRNA, with 25-35 modifications present in any one organism¹⁻⁴. In general, tRNA modifications enhance ribosome binding affinity, reduce misreading, and modulate frame-shifting, all of which affect the rate and fidelity of translation⁵⁻⁸. Emerging evidence points to a critical role for tRNA and rRNA modifications in the various cellular responses to stimuli, such as tRNA stability^{9,10}, transcription of stress response genes¹¹⁻¹³, and control of cell growth¹⁴.

We recently used high-throughput screens and targeted analyses to show that the tRNA methyltransferase 9 (Trm9) modulates the toxicity of methylmethanesulfonate (MMS) in *Saccharomyces cerevisiae*^{12,15}. This is similar to the observed role of Trm9 in modulating the toxicity of ionizing radiation¹⁶ and of Trm4 in promoting viability after methylation damage^{15,17}. Trm9 catalyzes the methyl esterification of the uracil-based cm⁵U and cm⁵s²U to mcm⁵U and mcm⁵s²U, respectively, at the wobble positions of tRNA^{UCU}-ARG and tRNA^{UUC}-GLU, among others¹⁸. These wobble base modifications enhance binding of the anticodon with specific codons in mixed codon boxes¹⁹. Codon-specific reporter assays and genome-wide searches revealed that Trm9-catalyzed tRNA modifications enhanced the translation of AGA- and GAA-rich transcripts that functionally mapped to processes associated with protein synthesis, metabolism, and stress signalling¹². These results lead to a model in which mRNA possessing specific codons will be more efficiently translated by tRNA with anticodons containing the Trm9-modified ribonucleoside and that tRNA modifications can dynamically change in response to stress.

To study the functional dynamics of this conserved system, we recently developed a bioanalytical platform to quantify the spectrum of ribonucleoside modifications and we used

it to assess the role of RNA modifications in the stress response of *S. cerevisiae*²⁰. This approach led to the discovery of signature changes in the spectrum of tRNA modifications in the cellular response to mechanistically different toxicants. Exposure of yeast to hydrogen peroxide (H₂O₂), as a model oxidative stressor, led to increases in the levels of 2'-*O*-methylcytosine (Cm), 5-methylcytosine (m⁵C), and *N*²,*N*²-dimethylguanosine (m²₂G), while these ribonucleosides decreased or were unaffected by exposure to MMS, arsenite, and hypochlorite²⁰. Loss of the methyltransferase enzymes catalyzing the formation of the modified ribonucleosides led to cytotoxic hypersensitivity to H₂O₂ exposure²⁰. These results support a general model of dynamic control of tRNA modifications in cellular response pathways and expand the repertoire of mechanisms controlling translational responses in cells.

In this present study we have used a variety of bioanalytical and bioinformatic approaches to define a step-wise mechanistic link between tRNA modifications and the oxidative stress response. Following an oxidative stress, reprogramming of a specific tRNA wobble modification leads to selective translation of mRNA species enriched with the cognate codon. Among the codon-biased, selectively translated proteins is one member of a pair of ribosomal protein paralogs, and the loss of this paralog causing sensitivity to oxidative stress. These results lead to a model in which stress-induced reprogramming of tRNA modifications and the associated reprogramming of ribosomes provides translational control of cell survival following an oxidative stress.

RESULTS

H₂O₂ increases m⁵C at the wobble position of tRNA^{Leu(CAA)}. In *S. cerevisiae*, m⁵C is synthesized by Trm4 methyltransferase (also called Ncl1) and we previously observed that the level of m⁵C in total tRNA increased following exposure to H₂O₂²⁰, with loss of Trm4 causing hypersensitivity to the cytotoxic effects of H₂O₂²⁰. To rule out second site mutations as the cause of this phenotype, we performed a complementation study using a *TRM4* expression vector in the *trm4* mutant strain and observed that re-expression of Trm4 conferred resistance to H₂O₂ exposure (Supplementary Figure S1 and Supplementary Methods).

Though m⁵C is present in at least 34 species of tRNA², tRNA^{Leu(CAA)} is the only tRNA with m⁵C at the anticodon wobble position 34, as well as position 48 at the junction between the variable and TΨC loops². To determine if H₂O₂ exposure altered the levels of m⁵C at one or both of these positions, tRNA^{Leu(CAA)} was purified from H₂O₂-exposed and unexposed cells by sequential gel and affinity purification. The resulting purified tRNA^{Leu(CAA)} was digested with RNase T1 to give a signature 4-mer oligoribonucleotide harboring either C or m⁵C at position 48 (CAAG) (Figure 1A). Additionally, total tRNA from H₂O₂-exposed and unexposed *S. cerevisiae* was digested with RNase U2 to produce another unique 5-mer oligoribonucleotide with C or m⁵C at position 34 of tRNA^{Leu(CAA)} (UUCAA) (Figure 1A). As shown in Figure 1B, subsequent mass spectrometric analysis of these oligonucleotides revealed that H₂O₂ exposure caused a 70% increase in m⁵C at the wobble position and a 20% decrease at position 48.

m⁵C controls the translation of UUG-enriched mRNA. Next we asked if the presence of m⁵C in tRNA^{Leu(CAA)} enhanced the translation of UUG-containing mRNA, given the evidence that m⁵C at the wobble position of the leucine-inserting amber suppressor tRNA^{Leu(CUA)} enhances translation²¹. To test this hypothesis, we used a dual Renilla and

Firefly luciferase reporter construct⁴² (illustrated in Figure 2A), in which the linker region connecting these two in-frame coding sequences was either four random or four TTG codons in a row (Control and 4X-TTG, respectively). Expression of the Firefly luciferase portion of the reporter fusion protein is thus dependent upon the efficiency of translating the linker region⁴². The expression of both the Renilla and Firefly luciferase reporters was quantified under conditions of oxidative stress and loss of Trm4 activity (Figures 2B, Supplementary Figure S2). As shown in Figure 2B, loss of Trm4 caused a 9.6-fold reduction in 4X-TTG reporter expression relative to wild-type cells under basal conditions. Following H₂O₂ treatment, there was an even larger 23.8-fold reduction in 4X-TTG reporter activity in *trm4Δ* cells compared to wild-type cells, with 4X-TTG reporter expression in wild-type cells unaffected by H₂O₂ exposure (Figure 2B). Effects of this magnitude were not observed for the control reporter, which was devoid of TTG codons in the linker region (Supplementary Figure S2). The *trm4Δ* cells containing the control reporter had an H₂O₂-induced 2-fold decrease in Firefly luciferase expression, relative to untreated cells, suggesting contributions by Trm4 to some aspect of general translation during oxidative stress. Taken together, these results are consistent with the idea that translation of TTG-rich sequences is facilitated by Trm4-catalyzed tRNA modifications and that m⁵C modifications play an important role in the translational response to H₂O₂ exposure. Coupled with the evidence for H₂O₂-induced increases in m⁵C at the wobble position of tRNA^{Leu(CAA)}, the data support a model in which oxidative stress causes a Trm4-mediated increase in the incorporation of m⁵C in tRNA^{Leu(CAA)}, with the methylated wobble base enhancing the translation of mRNA from genes enriched in TTG codon usage for leucine.

Differential codon enrichment in genes for ribosomal protein paralogs. This direct link between a tRNA wobble modification, codon usage and gene expression immediately raised the question of biases in the distribution of the TTG codon in genes that play a role in

responding to oxidative stress. Using a recently developed *S. cerevisiae* codon distribution database²², we quantified TTG codon use across the yeast genome. An average of 29% of leucines are coded by TTG in the 5782 genes analyzed. However, in 38 genes, more than 90% of the leucines are coded by TTG. Intriguingly, among these 38 genes, 26 encoded ribosomal proteins and the others are loosely related to energy metabolism (Table 1). These 26 ribosomal proteins represent a subset of the 138 such proteins encoded by the yeast genome. Of the 78 proteins that comprise a ribosome in *S. cerevisiae*, 59 occur in homologous pairs, or paralogs, that are believed to have arisen by an evolutionary genome duplication event²³. Recent evidence supports a model in which individual paralogs play different functional roles in a variety of cell processes in yeast²⁴⁻²⁷, with studies by Komili et al. revealing that a specific set of ribosomal protein homologs is necessary for the translation of *ASH1* mRNA during bud tip formation²⁸. One striking feature of the genes encoding paralogous ribosomal proteins is a bias in frequency of TTG codon use, as shown in Supplementary Tables S1 and S2. For example, 100% and 34% of the leucines in the paralogs Rpl22A and Rpl22B, respectively, are coded by TTG.

H₂O₂ increases a TTG-enriched ribosomal protein paralog. The biased distribution of TTG codons in ribosomal protein paralogs raised another question: will H₂O₂-induced increases in m⁵C in tRNA^{Leu(CAA)} lead to selective expression of TTG-enriched ribosomal protein paralogs? To test this hypothesis, we used a mass spectrometry-based proteomics approach to determine the relative quantities of several ribosomal protein paralogs in wild-type and *trm4Δ* mutant yeast exposed to H₂O₂²⁹. The study entailed isolation of polysomes from lysates of H₂O₂-treated and control yeast cells by differential ultracentrifugation, followed by trypsin digestion of the proteins and quantification of the tryptic peptides by liquid chromatography-coupled high-resolution mass spectrometry (LC-MS). Using this approach, we were able to consistently identify 39 ribosomal proteins in each of three

biological replicates (Supplementary Table S3), including seven pairs of distinguishable paralogs (Rpl6a/b, Rpl7a/b, Rpl16a/b, Rpl22a/b, Rpl33a/b, Rpl36a/b, and Rps7a/b) (Supplementary Tables S3, S4). Although the amino acid sequences of each set of paralogous proteins are nearly identical, they contain at least one signature tryptic peptide that could be used to identify and quantify each of 14 ribosomal paralogs in the mixture (Supplementary Table S4). A protein BLAST search in the NCBI database using these peptide sequences confirmed that the peptides were unique to the specific *S. cerevisiae* ribosomal proteins (data not shown). Further, the sequence identity of these unique peptides was confirmed by the analysis of the b- and y-ion series in collision-induced dissociation (CID) spectra (Supplementary Figure S3).

This approach was applied to determine the relative quantities of ribosomal homologs Rpl22a and Rpl22b, in which 100% and 34% of the leucines were coded by TTG, respectively. In the absence of absolute quantification of individual proteins, changes in the protein levels are expressed as changes in the ratio of the signals for the signature peptides from the protein pairs (e.g., Rpl22a/Rpl22b). The LC-MS signal ratios for the 14 ribosomal paralogs are shown in Supplementary Tables S5 and S6. A comparison of wild-type and *trm4* Δ mutants revealed that loss of *TRM4* caused a significant decrease in the ratio of Rpl22a to Rpl22b and of Rpl16b to Rpl16a (Figure 3), the two sets of paralogs with the largest differences in TTG codon use (Supplementary Table S4). When wild-type and *trm4* Δ cells were exposed to H₂O₂, the ratio of Rpl22a to Rpl22b increased significantly in the wild-type cells but not in the *trm4* mutants (Figure 4). To determine if these changes are indeed occurring at the level of translation, we quantified mRNA for both Rpl22a and Rpl22b by real-time quantitative PCR and we observed that the transcript levels remained unchanged following loss of *TRM4* or exposure to H₂O₂ (Supplementary Table S7).

H₂O₂ enhances translation of proteins with TTG-enriched genes. Having performed a targeted analysis of ribosomal proteins that revealed evidence of selective translation of TTG-enriched proteins, we next undertook a more general proteomic analysis of H₂O₂-induced differences in the ~200 most abundant proteins in yeast (Supporting Data 1), using a SILAC-based approach to quantify changes in the abundance of proteins in H₂O₂-induced cells⁴⁶. As shown in Figure 5, proteins with high TTG usage are more likely to be down-regulated (Figure 5A, $p = 0.048$ by Student's t-test) as a consequence of loss of Trm4 activity, while these proteins are significantly up-regulated in wild-type cells exposed to H₂O₂ (Figure 5B, $p = 6.41 \times 10^{-7}$). However, oxidative stress did not affect the expression of proteins from TTG-enriched genes in *trm4Δ* cells (Figure 5C, $p = 0.554$), which is consistent with a role for m⁵C in the selective translation of UUG-enriched mRNA species.

Analysis of the functional categories of proteins affected by H₂O₂ exposure (Supplementary Figure S4) reveals that proteins related to translation are significantly up-regulated by oxidative stress, which is consistent with the analysis of ribosomal protein expression in Figure 4, though Rpl22A and Rpl22B could not be differentiated likely as a result of the minimal sequence difference between the two proteins. One interesting complication apparent in Figure 5B is that proteins from genes with intermediate TTG frequencies (i.e., frequencies between the unchanged and up-regulated fractions) are significantly down-regulated in both H₂O₂ exposed wild-type cells ($p = 0.022$) and *trm4Δ* mutants ($p = 0.048$). This illustrates the limitations of our model for selective expression of TTG-enriched genes following oxidative stress and suggests that other layers of translational control are operant in the response to H₂O₂ exposure.

Rpl22A is required for the oxidative stress response in yeast. To further refine the mechanistic link between H₂O₂ exposure, m⁵C modification of tRNA, and Rpl22A expression as a survival response, we assessed the H₂O₂ sensitivity of yeast strains lacking

individual Rpl16A/B and Rpl22A/B paralogs²⁹. As shown in Figure 6 only the loss of *RPL22A* conferred sensitivity to H₂O₂, while the loss of *RPL16A*, *RPL16B* and *RPL22B* did not affect H₂O₂-induced cytotoxicity. The magnitude of the increased cytotoxicity caused by loss of Rpl22A (20% to 10% survival) is similar to the change in cytotoxicity that we observed previously for loss of Trm4²⁰. This suggests that Rpl22A contributes significantly to the oxidative stress survival response in yeast. The lack of effect of Rpl16b loss on H₂O₂ toxicity, in spite of the Trm4-dependence of this TTG-enriched paralog (Figure 3), suggests that it shares functional equivalence with Rpl16a in ribosomes.

DISCUSSION

Using a combination of bioanalytical and bioinformatic tools, we have defined a step-wise translational control mechanism responsible for cell survival following oxidative stress, a model for which is shown in Figure 7. While some of the individual steps in this model could be explained by other phenomena, such as tRNA or protein stability, there are few if any alternative mechanisms that could explain the sum of the observed behaviors. The first step in this model involves H₂O₂-induced increases in the level of m⁵C at the wobble position of tRNA^{Leu(CAA)} (Figure 7A) with a concomitant decrease in m⁵C at the neighboring position 48 in the same tRNA. The observation of a 70% increase in the proportion of tRNA^{Leu(CAA)} molecules containing a wobble m⁵C is consistent with a simple increase in TRM4 activity acting on a fixed concentration of total tRNA^{Leu(CAA)}. Alternatively, the proportion of m⁵C-containing tRNA^{Leu(CAA)} could remain constant, with an increase in transcription leading to an increase in the total number of copies of tRNA^{Leu(CAA)}, or both transcription and TRM4 activity could increase to raise the concentration of tRNA^{Leu(CAA)} with m⁵C. Finally, given the precedent for stress-induced degradation of tRNA^{9,10}, oxidative stress could lead to selective degradation of unmethylated tRNA^{Leu(CAA)}. By any mechanism, the data show that oxidative stress increases the proportion of tRNA^{Leu(CAA)} containing m⁵C at the wobble position, with an absolute requirement for Trm4 activity for the existence of m⁵C²⁰.

The second step in the model posits that the increase in m⁵C in tRNA^{Leu(CAA)} enhances the efficiency of translation of mRNAs enriched in the UUG codon recognized by this tRNA (Figure 7B). This is supported by the reporter assay results shown in Figure 2, with loss of Trm4 activity having no or little effect on reporter expression when TTG usage is low but causing a sharp decrease in expression when TTG usage is high. This is consistent with the observation that loss of Trm4, and thus m⁵C, decreases the expression of TTG-enriched

proteins but not unenriched proteins (Figures 3 and 5). The observation using the unmodified reporter (Supplementary Figure S2) that H₂O₂ exposure of wild-type cells did not affect reporter expression levels, yet it decreased reporter expression in the *trm4Δ* mutant, points to contributions by factors other than modification-specific codon usage in the control of translation during the oxidative stress response.

In addition to the proteome changes shown in Figure 5, the observed changes in expression of ribosomal proteins Rpl22A and Rpl16B (Figures 3 and 4) are consistent with the idea that oxidative stress enhances the translation of UUG-biased mRNAs. The pair of ribosomal gene parologs with the widest difference in the use of TTG for coding leucine, *RPL22A* at 100% and *RPL22B* at 38%, showed the largest changes in protein expression following H₂O₂ exposure, with expression of the high TTG-usage *RPL22A* increasing with oxidative stress and decreasing with loss of *TRM4* (Figure 4). The latter result points to the translational control of Rpl22A by Trm4, with the absolute requirement of oxidation-induced increases in m⁵C for the enhanced expression of Rpl22A. While we cannot rule out differential protein stability as a determinant of the proportions of the ribosomal protein paralog, differences in leucine content do not account for the differential stability of Rpl22A and Rpl22B. The paralog differ minimally in leucine content and the changes in paralog levels caused by loss of *TRM4* do not correlate with this amino acid. While Rpl22A and Rpl22B have 7 and 8 leucines, respectively, and the relative amount of Rpl22A decreases with loss of *TRM4*, Rpl16A and Rpl16B have 17 and 18 leucines, respectively, yet the relative quantity of *RPL16A* decreases with loss of *TRM4*. Further, the data presented here do not provide insights into the function of ribosomes with TTG-enriched ribosomal proteins, such as their potential role in selective translation of mRNAs enriched with TTG or other codons, or their possible role in the early and late stages of the oxidative stress response. A detailed analysis of ribosome-bound mRNAs or nascent peptides in the early and late stages

of the oxidative stress response would shed light on these issues. When considered with the other results, our observations suggest that the H₂O₂-induced increase in the level of the Rpl22a ribosomal protein is caused, at least in part, by Trm4-mediated changes in m⁵C levels in tRNA with subsequent control of translation of mRNA arising from TTG-enriched genes.

The mechanistic connection between Trm4 and Rpl22A is further established by the observation that loss of either protein makes corresponding *trm4*Δ²⁰ or *rpl22a*Δ (Figure 6) cells sensitive to H₂O₂. There are parallels for the H₂O₂-sensitive phenotype of *rpl22a*Δ in the recently defined roles of other ribosomal proteins in the oxidative stress response in higher eukaryotes. One example also serves as an illustration of the ribosome filter hypothesis concerning selective translation of mRNA³⁰: human ribosomal protein Rpl26 regulates translation of p53, a major node in oxidative stress response³¹, by interacting with the 5'-untranslated region of p53 mRNA³². Similarly, the highly conserved Rpl22³³ is involved in the activation of internal ribosomal entry site (IRES)-mediated translation in response to several types of stress^{34,35} and it participates in murine T-cell development by regulating translation of p53³⁶. Interestingly, ribosomal proteins may play roles in stress response other than ribosome structure, as suggested by recent observations of Rpl22 involvement in non-ribosomal ribonucleoprotein complexes such as the telomerase holoenzyme^{35,37-39}.

This series of observations leads to a model (Figure 7) in which oxidative stress causes an early increase in Trm4-mediated m⁵C levels in tRNA^{Leu(CAA)}, which leads to selective translation of UUG-enriched mRNAs, including ribosomal protein paralog Rpl22a and other proteins derived from many TTG-enriched genes. Clearly, this model does not address the complexity of translational control mechanisms, as suggested by the proteomic analysis shown in Figure 5, in which mRNA from genes with varying enrichment of TTG codons are not necessarily subject to enhanced translational efficiency. This complexity is further

illustrated by the possibility of reprogramming of other modifications, such as H₂O₂-induced increases in Cm and m²₂G²⁰, in other tRNA species, with subsequent selective expression of mRNAs enriched with other codons, as well as the potential for reprogramming of ribonucleoside modifications in rRNA species. Nonetheless, the present observations add to the growing recognition of a role for functional diversity in ribosome composition⁴⁰ and a role for ribosomes in selective translation of proteins³⁰. This reconfiguration of the translation machinery is similar to the proposed generation of “immunoribosomes” as a subset of T-cell ribosomes responsible for translating peptides involved in antigen presentation⁴¹. The abundance of ribosomal protein paralogs, the variety of RNA modifications in tRNA and rRNA, and the established biases in codon distributions in genes suggest a mechanism capable of fine tuning the translational response to virtually any cell stimulus.

METHODS

Codon reporter assay. The effect of TTG codon frequency on protein expression in wild-type and *trm4Δ* yeast cells was assessed using a dual luciferase reporter system⁴² in which Renilla luciferase is connected in-frame to Firefly luciferase by a 12 bp sequence (control: 5'-CCCGGGGAGCTC-3'; or 4X-TTG: 5'-TTGTTGTTGTTG-3'), all under the control of an ADH1 promoter and CYC1 terminator⁴². Following transformation with either control or 4X-TTG plasmid, cells were grown to $\sim 5 \times 10^6$ cells/mL and then treated with 2 mM H₂O₂ or H₂O for 60 min. Cells pellets were lysed by bead-beating in lysis buffer with and lysates clarified by centrifugation. Luminescence reactions were initiated with Promega DLR (50 μ L; Promega; Madison, WI) added to clarified lysates (5 μ L) and measured using a Victor Plate Reader (PerkinElmer; Waltham, MA).

RNase digestion of tRNA. Purified tRNA^{Leu(CAA)} (~ 2.5 μ g) was digested with RNase T1 (1 U; Ambion, Austin, TX) in 10 mM Tris buffer (pH 7.4, 37 °C, 1 hr). RNase U2 (Thermo Scientific, Waltham, MA) digestion (4 U) was carried out using total tRNA (0.5 mg, 37 °C, 4 hr). Oligoribonucleotides were dephosphorylated with alkaline phosphatase (10 U).

Quantifying m⁵C in tRNA^{Leu(CAA)}. RNase T1 and U2 digestion maps of tRNA were obtained using the Mongo Oligo Mass Calculator (v2.06; <http://library.med.utah.edu/masspec/mongo.htm>). Digested tRNA oligos were resolved by HPLC (C18 Hypersil GOLD aQ, 150 x 2.1 mm, 3 μ m particle; Thermo Scientific) coupled to a triple quadrupole mass spectrometer (MS) (6410; Agilent Technologies, Foster City, CA) with an electrospray ionization source operated in negative ion mode. HPLC was performed with a gradient of acetonitrile in 8 mM ammonium acetate (0.2 mL/min, 45 °C): 0-2 min, 1%; 2-30 min, 1-15%; 30-31 min, 15-100%; 31-41 min, 100%. MS parameters: drying gas, 325 °C and 8 L/min; nebulizer, 30 psi; capillary voltage, 3800 V; dwell time, 200 ms. The first

and third MS quadrupoles were set to unit resolution and the oligos containing m^5C were identified by comparison with standards and CID fragmentation patterns generated in a quadrupole time-of-flight MS. A selected ion chromatogram for a particular charge state of each oligo (unexposed and exposed to H_2O_2) was obtained, and the summation of the mass spectra over a particular peak was used for relative quantification of changes in m^5C levels at positions 34 and 48 of tRNA^{Leu}(^CAA).

Ribosome isolation. Cells (10^{10}) were resuspended in lysis buffer (10 mL) with 50 mM Tris-acetate, 50 mM ammonium chloride, 12 mM $MgCl_2$, and 1 mM dithiothreitol (pH 7) and lysed mechanically by bead-beating. Cell lysate was centrifuged (10000xg, 10 min), the supernatant collected, and centrifugation repeated twice to remove all particulates. The debris-free supernatant was layered over 2.5 mL of 1 M sucrose, 20 mM HEPES, 500 mM KCl, 2.5 mM magnesium acetate, and 2 mM dithiothreitol at pH 7.4 and centrifuged for 110 min at 370,000xg (r_{max}). Supernatant was removed and the pelleted ribosomes were resuspended in 1.5 mL of a digestion buffer with 100 mM ammonium acetate, pH 8.5. The samples were concentrated by spin dialysis on YM-10 filters. The concentrate was re-diluted with the digestion buffer and subject to spin dialysis five times to remove salts. Yield: ~300 μ g of protein.

Identification of ribosomal proteins. As the sequences of ribosomal protein paralogs are similar, we identified a unique tryptic peptide to quantify each paralog. Following reduction with dithiothreitol (1 mM, 2 hr, 37 °C) and alkylation with iodoacetamide (5.5 mM, 30 min, ambient temp.), purified ribosomal proteins (50 μ g) were digested with proteomics-grade trypsin (1 μ g) in 200 μ L of ammonium acetate solution (100 mM, pH 8.5, 37 °C, 12 h). Samples were lyophilized and resuspended in 100 μ L of 0.1% formic acid. Peptides in a portion of the tryptic digest (2.5 μ g, 5 μ L) were analyzed by LC-MS on an Agilent 1200 capillary HPLC coupled to an Agilent 6520 QTOF MS. Peptides were resolved on an

Agilent ZORBAX 300SB-C18 column (100 × 0.3 mm, 3 μm particle) eluted with a gradient of acetonitrile in 0.1% formic acid (20 μL/min, 45 °C): 0-25 min, 1-30%; 25-30 min, 30-60%; 30-31 min, 60-95%; 31-36 min, 95%. The MS was operated in positive ion mode with electrospray parameters as follows: fragmentor voltage, 110 V; drying gas, 300 °C and 5 L/min; nebulizer, 20 psi; capillary voltage, 3500 V. Peptide ions were scanned over m/z 100-1700 at an acquisition rate of 1.4 spectra/s. Data analysis was performed with Agilent Mass Hunter Software and compounds were detected using Molecular Feature Extractor (MFE) with 300 count minimum peak height and maximum charge state of 2. The MFE compound lists were subjected to peptide mass fingerprint analysis with the Agilent Spectrum Mill proteomics software to identify proteins based upon peptide accurate mass. A search was performed against the NCBI nr protein sequence database for *S. cerevisiae* with no protein modifications and missed cleavage considered, and with a 20 ppm mass tolerance and >25% protein coverage.

Identified peptides were sequenced by LC-QTOF using HPLC conditions described earlier and operating the QTOF in targeted MS/MS mode with acquisition rates for both MS and MS/MS scans at 1.4 spectra/s and a constant collision energy of 15 V to selectively monitor ions of the peptides shown in Supplementary Table S4; other MS parameters were described earlier. Peptide CID spectra were acquired by targeted MS/MS analysis and the b- and y-ion assignments (Supplementary Figure S3) used to determine the amino acid sequence. A search of the NCBI nr protein sequence database confirmed that each peptide uniquely identified its corresponding ribosomal protein paralog.

Relative quantification of ribosomal protein paralogs. With unique tryptic peptides for each paralog (Supplementary Table S4), the selected ion chromatogram of each peptide at charge state +2 was extracted from the total ion chromatogram, with the MS signal intensity determined by summation of the area under the mass spectrum (Supplementary Tables S5,

S6). Signal intensities for the ribosomal protein paralogs were normalized by taking their ratio, with the high TTG paralog in the numerator and low TTG in the denominator (Supplementary Tables S5, S6). This ratio was then used to determine changes in the quantities of ribosomal protein paralogs in H₂O₂-exposed cells (Figures 3, 4).

SILAC proteomics. *Lys1Δ* yeast cells were grown in yeast nitrogen base (YNB) medium containing 30 mg/L of L-lysine-U-[¹³C]₆, [¹⁵N]₂ (Isotec-SIGMA, Miamisburg, OH) for ≥10 generations, until they reached log-phase (OD₆₀₀ ~ 0.7)⁴³. Wild-type and *trm4Δ* yeast cells were grown in YNB medium containing 30 mg/L of L-lysine and were treated with 5 mM H₂O₂ at log-phase²⁰. Cells were harvested by centrifugation (1,500×g, 10 min, 4 °C), and washed twice with ice-cold H₂O. Cells were lysed by suspension in 2 M NaOH, 8% 2-mercaptoethanol v/v. Following TCA precipitation, proteins were pelleted by centrifugation (15,000×g, 15 min, 4 °C) and the pellet was resuspended in 8 M urea, 75 mM NaCl, 50 mM Tris, pH 8.2, 50 mM NaF, 50 mM β-glycerophosphate, 1 mM sodium orthovanadate, 10 mM sodium pyrophosphate, 1 mM PMSF⁴⁴. Protein concentration was determined by the Bradford assay⁴⁵. Heavy SILAC-labeled *lys1Δ* yeast proteins were used as a global internal standard⁴⁶. Following addition of internal standard to all treated and untreated wild-type and *trm4Δ* yeast protein samples (1:1), the protein mixture was reduced in 1mM dithiothreitol (2.5 hr, 37 °C), alkylated with iodoacetamide (5.5 mM, 40 min, ambient temp., dark), and then digested with 50:1 (w/w) trypsin (14 hr, 37 °C).

Peptide mixtures were loaded onto a Vydac C18 trap column (150 μm×10 mm, 5 μm/300 Å particle; Grace, Deerfield, IL) at 5 uL/min and eluted onto a Vydac C18 analytical column (75 μm×150 mm, 5 μm/300 Å particle) at 200 nL/min with a 120 min gradient of 2-98% acetonitrile in 0.1% formic acid. Eluted peptides were analyzed by MS analysis on a QSTAR-XL (Applied Biosystems, Foster City, CA). Acquired MS/MS spectra were parsed by Spectrum Mill and searched against Swiss-Prot database. CID spectra of tryptic peptides

were searched against the database sequences within a mass window of 100 ppm for precursor ion searches and 500 ppm for fragment ions. Database search results were filtered based on Spectrum Mill scoring criteria, which include peptide score, a measure of confidence of identification, and scored peak intensity (SPI) that represents the percentage of assigned peaks in CID spectrum. Peptide search results with a score ≥ 6 , SPI $\geq 60\%$ and no missed cleavages were used for protein quantification. SILAC peptide and protein quantification was performed with differential expression quantitation and SILAC protein ratios were determined as the average of all peptide ratios assigned to the protein. Differential protein expression was determined by Student's t-test for 4 biological replicates. A summary of identified proteins and their expression levels are presented in Supplementary Data 1.

Gene Ontology annotation. Gene functional categorization and pathway analysis were performed with DAVID Bioinformatics Resources 2011⁴⁷. The annotated proteins are clustered according to the biological process branch of the Gene Ontology (GO) annotation. The statistical significance of over-representation or under-representation of proteins in each GO category was assessed using a hypergeometric distribution and the significance indicated by the *p*-values for each GO category.

REFERENCES

- 1 Rozenski, J., Crain, P. F. & McCloskey, J. A. The RNA Modification Database: 1999 update. *Nucleic Acids Res* **27**, 196-197 (1999).
- 2 Czerwoniec, A. *et al.* MODOMICS: a database of RNA modification pathways. 2008 update. *Nucleic Acids Res* **37**, D118-121 (2009).
- 3 Söll, D. & RajBhandary, U. *tRNA: Structure, Biosynthesis and Function*. (ASM Press, 1995).
- 4 Limbach, P. A., Crain, P. F. & McCloskey, J. A. Summary: the modified nucleosides of RNA. *Nucleic Acids Res* **22**, 2183-2196 (1994).
- 5 Agris, P. F., Vendeix, F. A. & Graham, W. D. tRNA's wobble decoding of the genome: 40 years of modification. *J Mol Biol* **366**, 1-13 (2007).
- 6 Yarian, C. *et al.* Accurate translation of the genetic code depends on tRNA modified nucleosides. *J Biol Chem* **277**, 16391-16395 (2002).
- 7 Urbonavicius, J., Qian, Q., Durand, J. M., Hagervall, T. G. & Bjork, G. R. Improvement of reading frame maintenance is a common function for several tRNA modifications. *EMBO J* **20**, 4863-4873 (2001).
- 8 Bjork, G. R. *et al.* Transfer RNA modification: influence on translational frameshifting and metabolism. *FEBS Lett* **452**, 47-51 (1999).
- 9 Motorin, Y. & Helm, M. tRNA stabilization by modified nucleotides. *Biochemistry* **49**, 4934-4944 (2010).
- 10 Alexandrov, A. *et al.* Rapid tRNA decay can result from lack of nonessential modifications. *Mol Cell* **21**, 87-96 (2006).
- 11 Thompson, D. M. & Parker, R. Stressing out over tRNA cleavage. *Cell* **138**, 215-219 (2009).
- 12 Begley, U. *et al.* Trm9-catalyzed tRNA modifications link translation to the DNA damage response. *Mol Cell* **28**, 860-870 (2007).
- 13 Netzer, N. *et al.* Innate immune and chemically triggered oxidative stress modifies translational fidelity. *Nature* **462**, 522-526 (2009).

- 14 Emilsson, V., Naslund, A. K. & Kurland, C. G. Thiolation of transfer RNA in *Escherichia coli* varies with growth rate. *Nucleic Acids Res* **20**, 4499-4505 (1992).
- 15 Begley, T. J., Rosenbach, A. S., Ideker, T. & Samson, L. D. Hot spots for modulating toxicity identified by genomic phenotyping and localization mapping. *Mol Cell* **16**, 117-125 (2004).
- 16 Bennett, C. B. *et al.* Genes required for ionizing radiation resistance in yeast. *Nat Genet* **29**, 426-434. (2001).
- 17 Rooney, J. P. *et al.* Systems based mapping demonstrates that recovery from alkylation damage requires DNA repair, RNA processing, and translation associated networks. *Genomics* **10**, 524 (2008).
- 18 Kalhor, H. R. & Clarke, S. Novel methyltransferase for modified uridine residues at the wobble position of tRNA. *Mol Cell Biol* **23**, 9283-9292 (2003).
- 19 Weissenbach, J. & Dirheimer, G. Pairing properties of the methylester of 5-carboxymethyl uridine in the wobble position of yeast tRNA^{3Arg}. *Biochim Biophys Acta* **518**, 530-534 (1978).
- 20 Chan, C. T. *et al.* A quantitative systems approach reveals dynamic control of tRNA modifications during cellular stress. *PLoS Genetics* **6**, e1001247 (2010).
- 21 Strobel, M. C. & Abelson, J. Effect of intron mutations on processing and function of *Saccharomyces cerevisiae* SUP53 tRNA in vitro and in vivo. *Mol Cell Biol* **6**, 2663-2673 (1986).
- 22 Tumu, S., Patil, A., Towns, W., Dyavaiah, M. & Begley, T. J. The Gene Specific Codon Usage Database: A genome-based catalog of one, two, three, four and five codon combinations present in *Saccharomyces cerevisiae* genes. *Database* 2012:bas002 (2012).
- 23 Kellis, M., Birren, B. W. & Lander, E. S. Proof and evolutionary analysis of ancient genome duplication in the yeast *Saccharomyces cerevisiae*. *Nature* **428**, 617-624 (2004).

- 24 Baudin-Baillieu, A., Tollervey, D., Cullin, C. & Lacroute, F. Functional analysis of Rrp7p, an essential yeast protein involved in pre-rRNA processing and ribosome assembly. *Mol Cell Biol* **17**, 5023-5032 (1997).
- 25 Enyenihi, A. H. & Saunders, W. S. Large-scale functional genomic analysis of sporulation and meiosis in *Saccharomyces cerevisiae*. *Genetics* **163**, 47-54 (2003).
- 26 Haarer, B., Viggiano, S., Hibbs, M. A., Troyanskaya, O. G. & Amberg, D. C. Modeling complex genetic interactions in a simple eukaryotic genome: actin displays a rich spectrum of complex haploinsufficiencies. *Genes Dev* **21**, 148-159 (2007).
- 27 Ni, L. & Snyder, M. A genomic study of the bipolar bud site selection pattern in *Saccharomyces cerevisiae*. *Mol Biol Cell* **12**, 2147-2170 (2001).
- 28 Komili, S., Farny, N. G., Roth, F. P. & Silver, P. A. Functional specificity among ribosomal proteins regulates gene expression. *Cell* **131**, 557-571 (2007).
- 29 VanDyke & Dervan. Echinomycin binding sites on DNA. *Science* **225**, 1122-1127 (1984).
- 30 Mauro, V. P. & Edelman, G. M. The ribosome filter redux. *Cell Cycle* **6**, 2246-2251 (2007).
- 31 Liu, D. & Xu, Y. p53, Oxidative Stress, and Aging. *Antioxid Redox Signal* **15**, 1669-1678 (2011).
- 32 Takagi, M., Absalon, M. J., McLure, K. G. & Kastan, M. B. Regulation of p53 translation and induction after DNA damage by ribosomal protein L26 and nucleolin. *Cell* **123**, 49-63 (2005).
- 33 Nakao, A., Yoshihama, M. & Kenmochi, N. RPG: the Ribosomal Protein Gene database. *Nucleic Acids Res* **32**, D168-170 (2004).
- 34 Holcik, M. & Sonenberg, N. Translational control in stress and apoptosis. *Nat Rev Mol Cell Biol* **6**, 318-327 (2005).
- 35 Wood, J., Frederickson, R. M., Fields, S. & Patel, A. H. Hepatitis C virus 3'X region interacts with human ribosomal proteins. *J Virol* **75**, 1348-1358 (2001).

- 36 Anderson, S. J. *et al.* Ablation of ribosomal protein L22 selectively impairs alphabeta T cell development by activation of a p53-dependent checkpoint. *Immunity* **26**, 759-772 (2007).
- 37 Dobbstein, M. & Shenk, T. In vitro selection of RNA ligands for the ribosomal L22 protein associated with Epstein-Barr virus-expressed RNA by using randomized and cDNA-derived RNA libraries. *J Virol* **69**, 8027-8034 (1995).
- 38 Le, S., Sternglanz, R. & Greider, C. W. Identification of two RNA-binding proteins associated with human telomerase RNA. *Mol Biol Cell* **11**, 999-1010 (2000).
- 39 Toczyski, D. P. & Steitz, J. A. EAP, a highly conserved cellular protein associated with Epstein-Barr virus small RNAs (EBERs). *EMBO J* **10**, 459-466 (1991).
- 40 Dlakic, M. The ribosomal subunit assembly line. *Genome Biol* **6**, 234 (2005).
- 41 Yewdell, J. W. & Nicchitta, C. V. The DRiP hypothesis decennial: support, controversy, refinement and extension. *Trends Immunol* **27**, 368-373 (2006).
- 42 Plant, E. P. *et al.* Differentiating between near- and non-cognate codons in *Saccharomyces cerevisiae*. *PLoS One* **2**, e517 (2007).
- 43 de Godoy, L. M. *et al.* Comprehensive mass-spectrometry-based proteome quantification of haploid versus diploid yeast. *Nature* **455**, 1251-1254 (2008).
- 44 Gruhler, A. *et al.* Quantitative phosphoproteomics applied to the yeast pheromone signaling pathway. *Mol Cell Proteomics* **4**, 310-327 (2005).
- 45 Bradford, M. M. A rapid and sensitive method for the quantitation of microgram quantities of protein utilizing the principle of protein-dye binding. *Anal Biochem* **72**, 248-254 (1976).
- 46 Ishihama, Y. *et al.* Quantitative mouse brain proteomics using culture-derived isotope tags as internal standards. *Nat Biotechnol* **23**, 617-621 (2005).
- 47 Huang da, W., Sherman, B. T. & Lempicki, R. A. Systematic and integrative analysis of large gene lists using DAVID bioinformatics resources. *Nat Protoc* **4**, 44-57 (2009).

ACKNOWLEDGEMENTS

The authors thank Prof. Wendy Gilbert (Dept. of Biology, MIT) for assistance with ribosome purification. We also thank Drs. Koli Taghizadeh and John Wishnok for assistance with mass spectrometry, which was performed in the Bioanalytical Facilities Core of the MIT Center for Environmental Health Sciences. Financial support was provided by the National Institute of Environmental Health Sciences (ES002109, ES017010, ES015037 and ES017010), the MIT Westaway Fund, a Merck–MIT Graduate Student Fellowship (C.T.Y.C.) and the Singapore-MIT Alliance for Research and Technology. The authors declare no competing financial interests.

AUTHOR CONTRIBUTIONS

The authors contributed to (A) experimental design, (B) performance of experiments, (C) data analysis and interpretation, (D) preparation of the manuscript as follows:

Clement T. Y. Chan A, B, C, D

Yan Ling Joy Pang A, B, C, D

Wenjun Deng A, B, C, D

I. Ramesh Babu A, C, D

Madhu Dyavaiah A, B, C, D

Thomas J. Begley A, C, D

Peter C. Dedon A, C, D

TABLES

Table 1. *S. cerevisiae* genes with $\geq 90\%$ TTG codon usage for leucine.

Gene Name	#TTG	Freq. of TTG ¹	Protein Function
<i>RPL15A</i>	13	1	Protein component of the large (60S) ribosomal subunit
<i>RPL28</i>	9	1	Ribosomal protein of the large (60S) ribosomal subunit
<i>RPL39</i>	2	1	Protein component of the large (60S) ribosomal subunit
<i>RPS10B</i>	9	1	Protein component of the small (40S) ribosomal subunit
<i>CCW12</i>	9	1	Cell wall mannoprotein
<i>RPL22A</i>	7	1	Protein component of the large (60S) ribosomal subunit
<i>RPL43A</i>	3	1	Protein component of the large (60S) ribosomal subunit
<i>RPL37B</i>	2	1	Protein component of the large (60S) ribosomal subunit
<i>RPL37A</i>	2	1	Protein component of the large (60S) ribosomal subunit
<i>HYP2</i>	11	1	Translation elongation factor eIF-5A
<i>RPS15</i>	9	1	Protein component of the small (40S) ribosomal subunit
<i>RPL36B</i>	6	1	Protein component of the large (60S) ribosomal subunit
<i>NOP10</i>	5	1	Constituent of small nucleolar ribonucleoprotein particles
<i>RPS26B</i>	4	1	Protein component of the small (40S) ribosomal subunit
<i>HSP12</i>	3	1	Plasma membrane localized protein
<i>TDH3</i>	20	0.95	Glyceraldehyde-3-phosphate dehydrogenase, isozyme 3
<i>TDH2</i>	20	0.95	Glyceraldehyde-3-phosphate dehydrogenase, isozyme 2
<i>TDH1</i>	19	0.95	Glyceraldehyde-3-phosphate dehydrogenase, isozyme 1
<i>RPL8A</i>	19	0.95	Ribosomal protein L4 of the large (60S) ribosomal subunit
<i>RPS6B</i>	19	0.95	Protein component of the small (40S) ribosomal subunit
<i>RPS6A</i>	19	0.95	Protein component of the small (40S) ribosomal subunit
<i>RPL10</i>	16	0.94	Protein component of the large (60S) ribosomal subunit
<i>RPL4A</i>	26	0.93	Protein component of the large (60S) ribosomal subunit
<i>RPL4B</i>	26	0.93	Protein component of the large (60S) ribosomal subunit
<i>RPS13</i>	13	0.93	Protein component of the small (40S) ribosomal subunit
<i>RPS5</i>	13	0.93	Protein component of the small (40S) ribosomal subunit
<i>ENO2</i>	35	0.92	Enolase II
<i>ANB1</i>	11	0.92	Translation elongation factor eIF-5A
<i>CDC19</i>	32	0.91	Pyruvate kinase
<i>RPL12B</i>	10	0.91	Protein component of the large (60S) ribosomal subunit
<i>PDC1</i>	49	0.91	Major of three pyruvate decarboxylase isozymes
<i>RPS2</i>	19	0.90	Protein component of the small (40S) subunit
<i>RPL8B</i>	19	0.90	Ribosomal protein L4 of the large (60S) ribosomal subunit
<i>ENO1</i>	36	0.90	Enolase I
<i>RPL17A</i>	9	0.90	Protein component of the large (60S) ribosomal subunit
<i>RPL17B</i>	9	0.90	Protein component of the large (60S) ribosomal subunit
<i>RPS9B</i>	18	0.90	Protein component of the small (40S) ribosomal subunit
<i>RPL9A</i>	9	0.90	Protein component of the large (60S) ribosomal subunit

¹Proportion of leucines encoded by TTG

FIGURE LEGENDS

Figure 1. H₂O₂ exposure increases the level of m⁵C at the wobble position of tRNA^{Leu(CAA)}.

(A) tRNA^{Leu(CAA)} was digested with ribonucleases to generate oligoribonucleotides containing m⁵C or C at position 34 (CAAG) or position 48 (UUCAA), and the oligoribonucleotides were quantified by mass spectrometry. (B) The graph shows the ratio of m⁵C/C in tRNA^{Leu(CAA)} from H₂O₂-treated cells relative to untreated cells. The data represent mean ± SD for three experiments. The data for position 34 are significantly different from those for position 48 by Student's t-test with $p < 0.05$.

Figure 2. H₂O₂ and Trm4 methyltransferase control gene expression at the level of TTG codon usage. (A) Scheme illustrating the dual luciferase reporter system for assessing the effect of TTG codon usage on protein expression in wild-type and *trm4Δ* mutant yeast cells transformed with either control or 4X-TTG reporter plasmids. (B) Control and 4X-TTG reporter activity was quantified in H₂O₂-exposed (gray bars) and unexposed (white bars) wild-type or *trm4Δ* cells. The ratio of treated to untreated is indicated above each condition. Data represent mean ± deviation about the mean for three biological replicates.

Figure 3. Loss of Trm4 methyltransferase decreases the proportion of ribosomes containing TTG codon-enriched ribosomal protein paralogs. Ribosomal proteins in wild-type and *trm4Δ* mutant *S. cerevisiae* were quantified by LC-MS/MS (schematic inset) and the relative quantities of ribosomal protein paralogs presented as the ratio of the signal intensity for the paralog with high TTG-usage to that of the low-usage paralog. Data represent mean ± SD for three biological replicates. p values denote statistically significant differences by Student's t-test.

Figure 4. H₂O₂ exposure increases the proportion of ribosomes containing ribosomal protein paralog Rpl22a in wild-type *S. cerevisiae* but not *trm4Δ* mutants. Cells were exposed to 2 mM H₂O₂ for 1 hr and the quantities of ribosomal proteins were determined by LC-MS/MS analysis. Data are expressed as the ratio of the TTG-enriched paralog Rpl22a to unenriched Rpl22b. Data represent mean ± SD of three biological replicates. Asterisks denote statistically significant differences between H₂O₂-treated and untreated cells as judged by Student's t-test with $p < 0.05$.

Figure 5. SILAC-based proteomic analysis reveals that H₂O₂ enhances the translation of TTG-enriched proteins. Protein extracts from control and H₂O₂-treated wild-type and *trm4* mutant yeast were mixed 1:1 with proteins from U-[¹³C, ¹⁵N]-lysine-labeled *lys1Δ* yeast cells as an internal standard⁴⁶. Protein mixtures were then subjected to trypsin digestion and proteomic analysis by LC-QTOF analysis. The quantities of the 261 most abundant proteins appearing in each of four biological replicates were analyzed by Student's t-test ($p < 0.05$) for increased (up-regulation), decreased (down-regulation) or unchanged levels in H₂O₂-treated versus control cells, or wild-type versus *trm4Δ* mutant. Within these three groups of proteins, the frequency of using TTG to code for leucine was calculated. The resulting frequency data are presented as a box-and-whiskers plot with the bar representing the median value, the box encompassing the range of data between the first and third quartile, and the error bars embracing data within 1.5-times interquartile range. Differences between up-regulated, down-regulated and unchanged categories were subjected to Student's t-test with the indicated p values.

Figure 6. Ribosomal protein paralog Rpl22a confers resistance to H₂O₂ exposure in *S. cerevisiae*. Wild-type *S. cerevisiae* and strains lacking *RPL16A*, *RPL16B*, *RPL22A*, or

RPL22B were exposed to 5 mM H₂O₂ and survival was assayed as described in Methods. Data represent mean \pm SD of three biological replicates. The asterisk denotes a statistically significant difference compared to all other values in the figure, as judged by Student's t-test with $p < 0.05$.

Figure 7. Proposed mechanism by which increase in m⁵C level regulates translation of ribosomal protein paralogs and confers resistance to H₂O₂. Exposure to H₂O₂ leads to an elevation in the level of m⁵C at the wobble position of the leucine tRNA for translating the codon UUG on mRNA (**A**), which enhances the translation of the UUG-enriched *RPL22A* mRNA relative to its paralog *RPL22B* (**B**) and leads to changes in ribosome composition (**C**). This reprogramming of tRNA and ribosomes ultimately causes selective translation of proteins from genes enriched with the codon TTG.

FIGURES

Figure 1

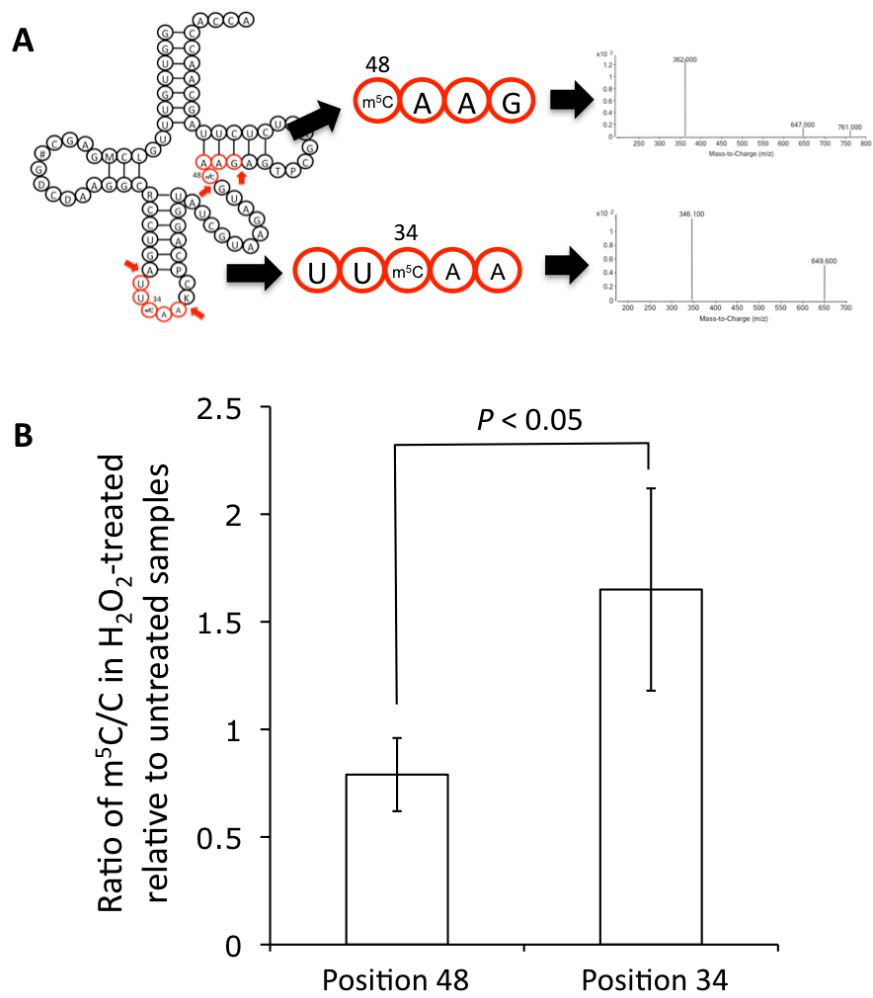


Figure 2

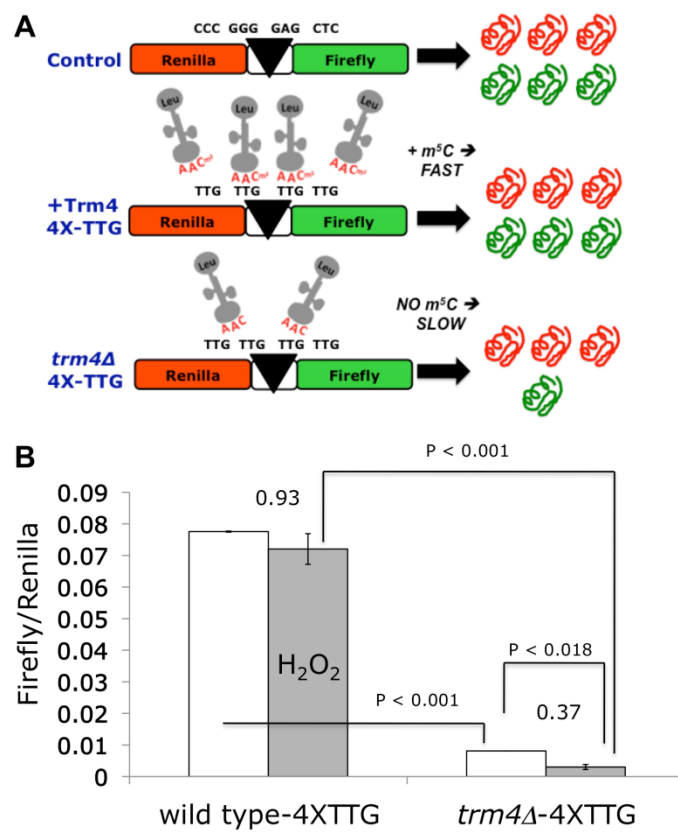


Figure 3

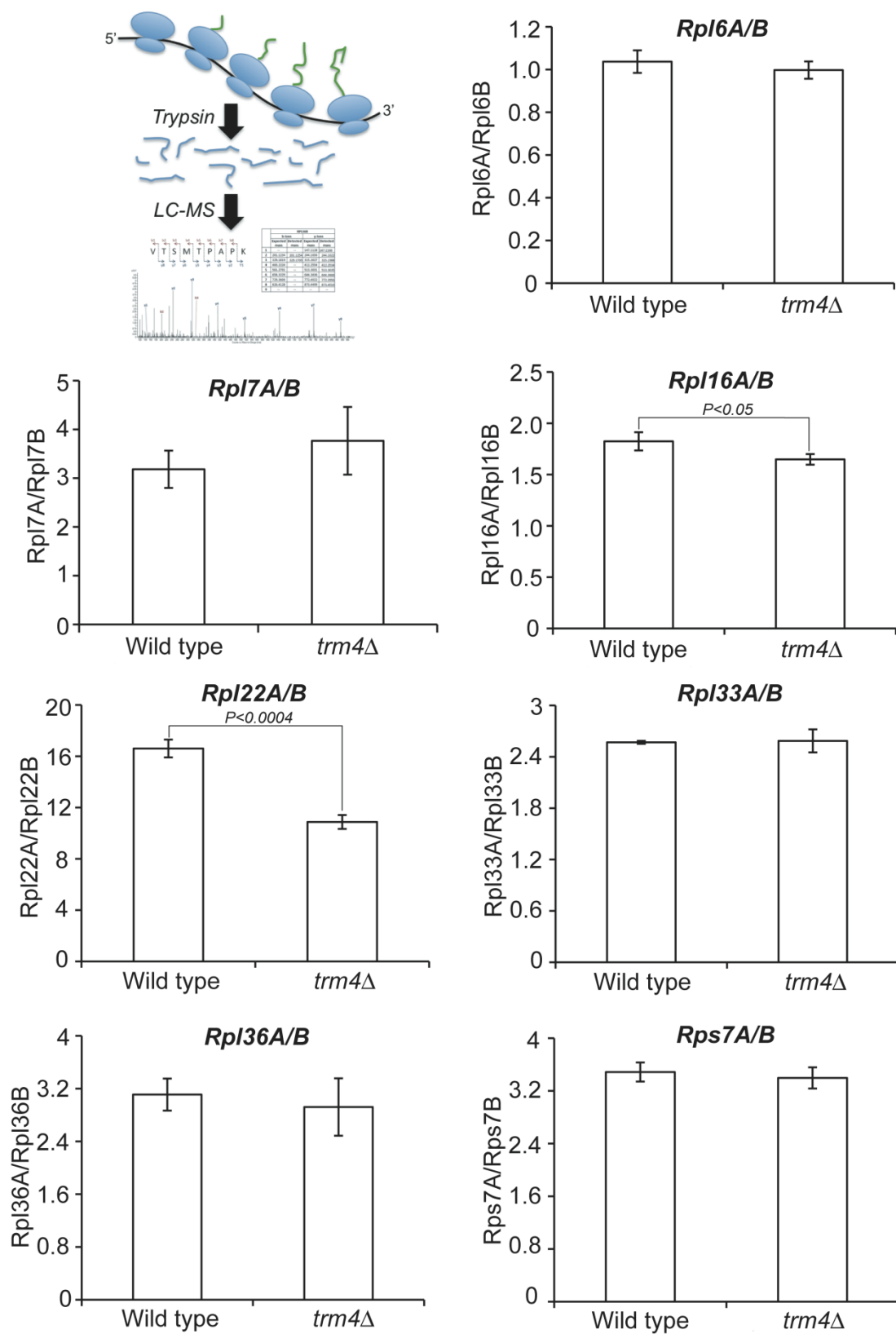


Figure 4

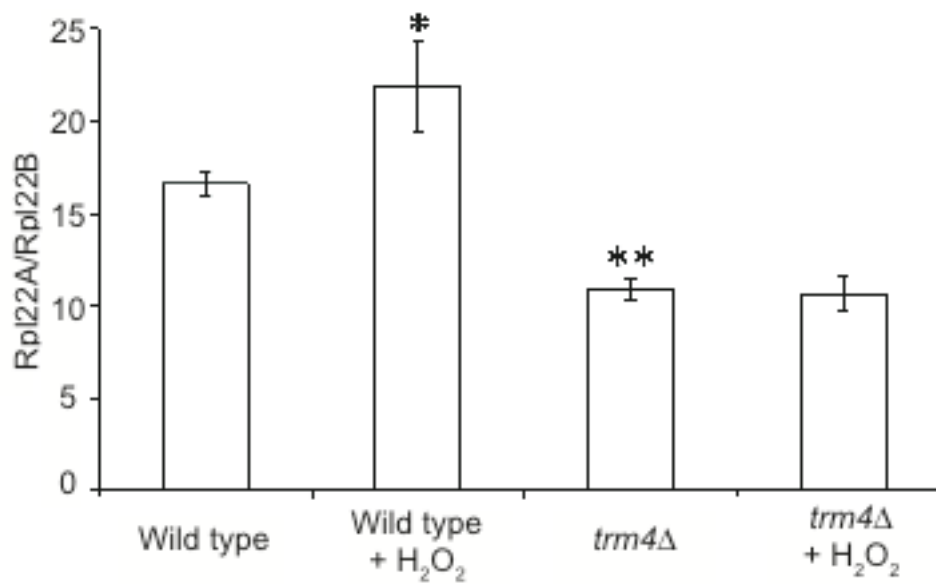


Figure 5

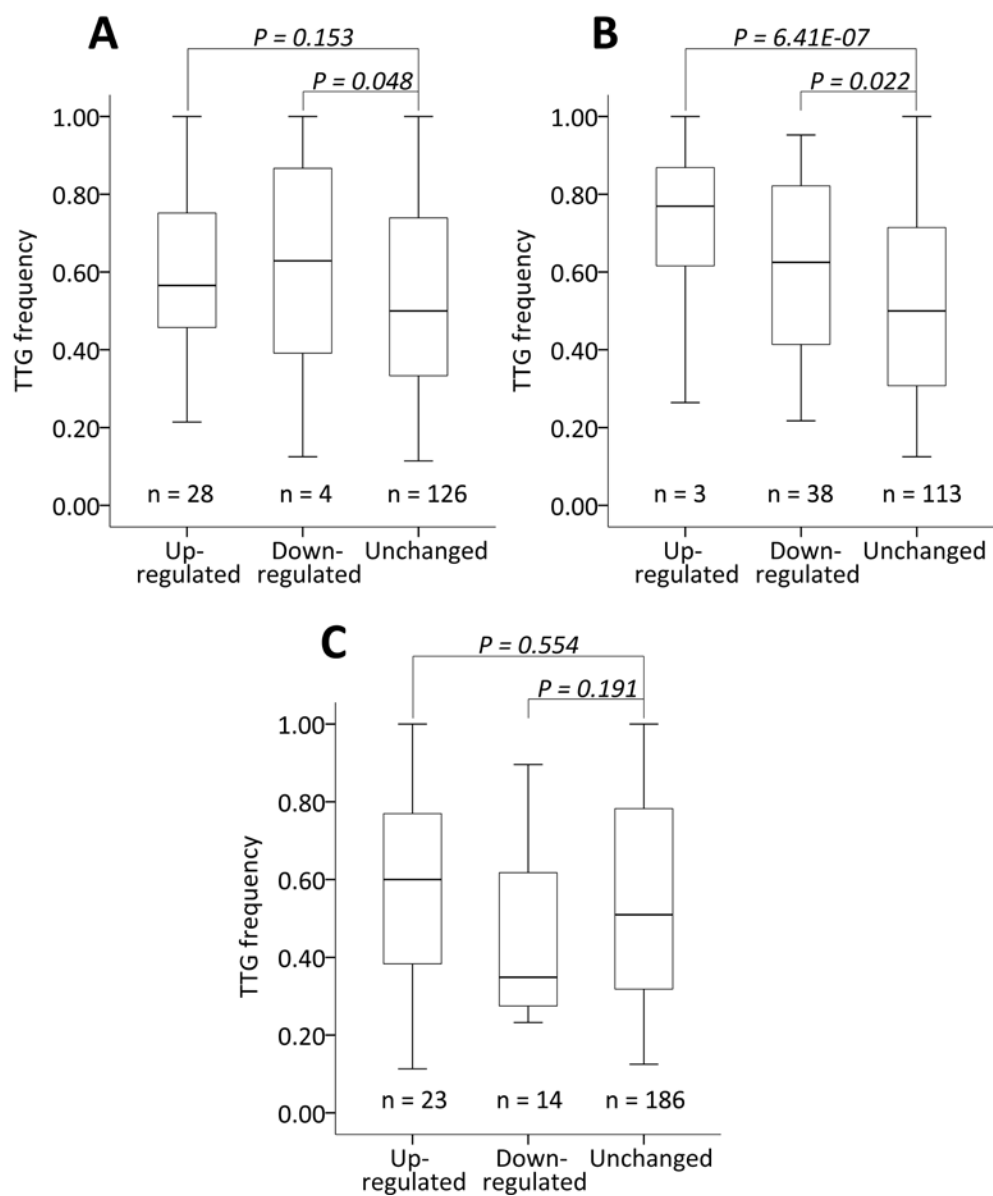


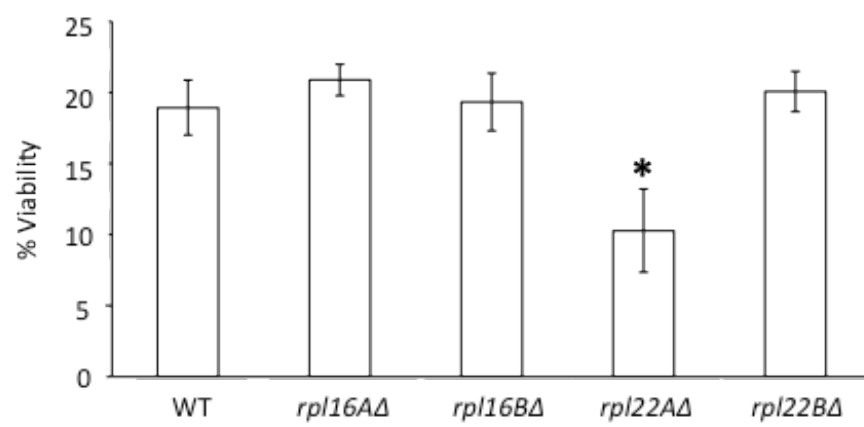
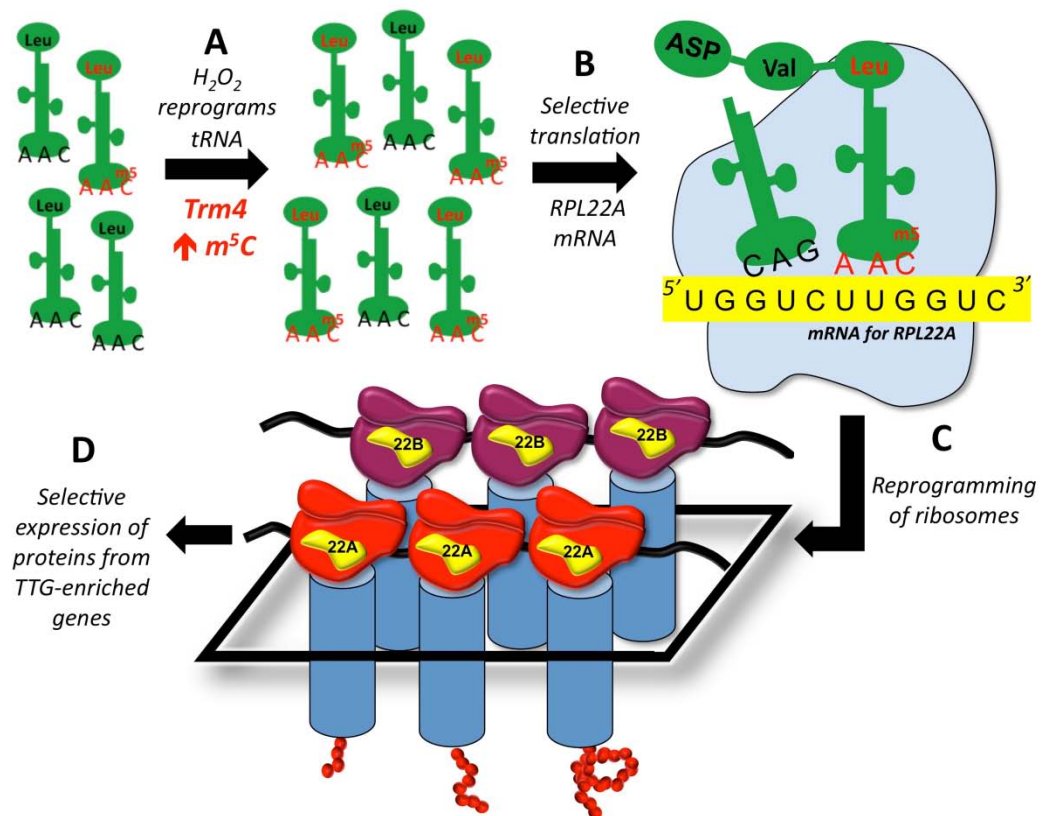
Figure 6

Figure 7



SUPPLEMENTARY INFORMATION

“Reprogramming of tRNA modifications controls the oxidative stress response by codon-biased translation of proteins,” by Clement T.Y. Chan, Yan Ling Joy Pang, Wenjun Deng, I. Ramesh Babu, Madhu Dyavaiah, Thomas J. Begley and Peter C. Dedon

SUPPLEMENTARY TABLES

Supplementary Table S1: TTG codon usage in *S. cerevisiae* genes for large ribosomal subunit proteins.

Gene Name	#TTG	TTG frequency	Δ#TTG	Gene Name	#TTG	TTG frequency	Δ#TTG
RPL1A	22	0.88	0	RPL23A	5	0.56	1
RPL1B	22	0.88		RPL23B	4	0.44	
RPL2A	13	0.81	3	RPL24A	6	0.86	0
RPL2B	10	0.63		RPL24B	6	0.86	
RPL3	18	0.86	--	RPL25	9	0.82	--
RPL4A	26	0.93	0	RPL26A	9	0.64	0
RPL4B	26	0.93		RPL26B	9	0.64	
RPL5	17	0.74	--	RPL27A	5	0.71	0
RPL6A	13	0.68	2	RPL27B	5	0.83	
RPL6B	15	0.75		RPL28	9	1.00	--
RPL7A	17	0.85	0	RPL29	2	0.67	--
RPL7B	17	0.85		RPL30	11	0.85	--
RPL8A	19	0.95	0	RPL31A	6	0.55	0
RPL8B	19	0.90		RPL31B	6	0.55	
RPL9A	9	0.90	1	RPL32	7	0.78	--
RPL9B	8	0.89		RPL33A	5	0.83	1
RPL10	16	0.94	--	RPL33B	4	0.67	
RPL11A	8	0.73	1	RPL34A	4	0.80	0
RPL11B	7	0.64		RPL34B	4	0.80	
RPL12A	6	0.55	4	RPL35A	11	0.85	1
RPL12B	10	0.91		RPL35B	10	0.77	
RPL13A	5	0.45	4	RPL36A	4	0.67	2
RPL13B	9	0.82		RPL36B	6	1.00	
RPL14A	7	0.64	0	RPL37A	2	1.00	0
RPL14B	7	0.64		RPL37B	2	1.00	
RPL15A	13	1.00	5	RPL38	8	0.89	--
RPL15B	8	0.62		RPL39	2	1.00	--
RPL16A	9	0.50	5	RPL40A	12	0.86	2
RPL16B	14	0.82		RPL40B	10	0.71	
RPL17A	9	0.90	0	RPL41A	0	0.00	0
RPL17B	9	0.90		RPL41B	0	0.00	
RPL18A	11	0.73	1	RPL42A	7	1.00	1
RPL18B	10	0.67		RPL42B	6	0.86	
RPL19A	9	0.56	1	RPL43A	3	1.00	2
RPL19B	10	0.63		RPL43B	1	0.33	
RPL20A	8	0.89	2	RPP0	21	0.84	--
RPL20B	6	0.60		RPP1A	9	0.82	5
RPL21A	4	0.50	2	RPP1B	4	0.50	
RPL21B	6	0.86		RPP2A	5	0.50	0
RPL22A	7	1.00	4	RPP2B	5	0.56	
RPL22B	3	0.38					

Supplementary Table S2: Usage of the TTG codon in *S. cerevisiae* genes for proteins in the small ribosomal subunit.

Gene Name	#TTG	TTG frequency	Δ #TTG	Gene Name	#TTG	TTG frequency	Δ #TTG
RPS0A	9	0.47	5	RPS17A	13	0.87	0
RPS0B	14	0.70		RPS17B	13	0.87	
RPS1A	16	0.73	3	RPS18A	11	0.73	1
RPS1B	19	0.83		RPS18B	10	0.67	
RPS2	19	0.90	--	RPS19A	6	0.75	1
RPS3	12	0.63	--	RPS19B	7	0.88	
RPS4A	16	0.64	2	RPS20	5	0.83	--
RPS4B	18	0.72		RPS21A	4	0.57	1
RPS5	13	0.93	--	RPS21B	5	0.71	
RPS6A	19	0.95	0	RPS22A	8	0.80	2
RPS6B	19	0.95		RPS22B	6	0.55	
RPS7A	18	0.86	4	RPS23A	10	0.77	0
RPS7B	14	0.67		RPS23B	10	0.77	
RPS8A	5	0.50	0	RPS24A	3	0.18	3
RPS8B	5	0.50		RPS24B	6	0.67	
RPS9A	12	0.60	6	RPS25A	4	0.44	2
RPS9B	18	0.90		RPS25B	6	0.67	
RPS10A	7	0.78	2	RPS26A	2	0.50	2
RPS10B	9	1.00		RPS26B	4	1.00	
RPS11A	3	0.60	0	RPS27A	3	0.33	2
RPS11B	3	0.60		RPS27B	5	0.56	
RPS12	11	0.73	--	RPS28A	3	0.50	1
RPS13	13	0.93	--	RPS28B	4	0.67	
RPS14A	4	0.67	0	RPS29A	1	0.50	0
RPS14B	4	0.57		RPS29B	1	0.50	
RPS15	9	1.00	--	RPS30A	2	0.50	0
RPS16A	7	0.64	1	RPS30B	2	0.50	
RPS16B	8	0.73		RPS31	11	0.79	--

Supplementary Table S3. Ribosomal proteins consistently identified by LC-MS/MS analysis of signature peptides from trypsinized polysomal proteins in three biological replicates. The table shows the percentage of the protein sequence coverage as represented by the detected peptides and the average errors in peptide mass measurements compared to the theoretical values.

Proteins	Protein Sequence Coverage (%)			Mass Error Mean (Std. Dev.), ppm		
	Expt. 1	Expt. 2	Expt. 3	Expt. 1	Expt. 2	Expt. 3
Rpl2b	46	38	40	-5.5 (5.8)	-5.3 (6.4)	-6.1 (6.3)
Rpl6a	37	40	32	1.2 (6.1)	-3.3 (6.6)	-2.7 (7.3)
Rpl6b	48	44	36	-5.9 (5.9)	-3.1 (4.7)	-2.1 (7.0)
Rpl7a	40	35	40	1.1 (6.5)	-1.8 (4.5)	-2.5 (7.0)
Rpl7b	40	35	40	0.8 (6.6)	-2.0 (4.6)	-2.8 (7.1)
Rpl9a/b	50	41	41	-2.1 (8.2)	-3.3 (8.3)	-3.1 (10.7)
Rpl11a/b	28	31	25	1.5 (3.2)	-0.9 (4.4)	-1.8 (2.6)
Rpl15a	31	33	33	0.3 (2.3)	2.3 (6.5)	-0.3 (8.6)
Rpl16a	44	37	44	-2.6 (8.7)	-2.5 (8.4)	-2.1 (7.6)
Rpl16b	45	42	39	-1.8 (8.5)	-3.9 (8.3)	-3.8 (8.6)
Rpl18b	41	38	46	-1.3 (8.2)	-2.5 (8.3)	-2.4 (7.0)
Rpl19b	29	32	63	-4.3 (6.3)	-2.7 (9.3)	-4.4 (7.3)
Rpl20a	51	47	48	1.8 (7.3)	1.9 (7.3)	-0.6 (5.1)
Rpl21a/b	46	46	46	-3.7 (4.8)	-3.2 (6.1)	-2.4 (5.5)
Rpl22a	35	68	54	1.7 (12.3)	0.2 (6.6)	3.3 (9.4)
Rpl22b	49	50	50	0.2 (5.8)	1.1 (6.2)	1.8 (10.8)
Rpl23a	55	48	55	-0.4 (6.6)	-0.5 (9.4)	-1.1 (8.0)
Rpl27a	46	46	43	-0.4 (9.4)	-2.6 (8.7)	-4.4 (6.5)
Rpl32	46	56	53	0.1 (4.2)	0.5 (6.2)	-1.2 (1.2)
Rpl33a	49	44	49	0.7 (8.8)	-5.3 (10.2)	-0.8 (8.5)
Rpl33b	49	44	49	0.7 (8.8)	-5.3 (10.2)	-0.8 (8.5)
Rpl35b	30	37	37	-0.3 (6.2)	-4.8 (5.0)	-4.2 (5.5)
Rpl36a	52	52	39	-5.3 (5.7)	-2.4 (8.3)	-0.1 (1.9)
Rpl36b	52	52	52	-4.8 (6.1)	-2.0 (8.4)	-4.8 (6.1)
Rps1a/b	45	36	36	1.4 (7.5)	-4.0 (5.6)	-0.9 (5.9)
Rps2	38	38	36	-0.4 (10)	-4.7 (4.5)	-1.6 (8.7)
Rps3	48	56	56	-2.7 (4.7)	-3.5 (4.8)	-4.0 (4.5)
Rps4a/b	59	57	63	-1.5 (8.3)	-2.1 (8.2)	-3.7 (9.3)
Rps7a	64	64	66	-0.5 (5.8)	-1.5 (7.0)	-2.5 (7.1)
Rps7b	68	64	66	-2.3 (6.6)	-5.1 (6.6)	-5.6 (6.6)
Rps9a/b	54	54	54	-0.5 (7.5)	-1.4 (7.2)	-1.8 (6.9)
Rps13	68	62	58	-2.1 (4.0)	-2.8 (5.8)	-3.5 (3.7)
Rps17a/b	62	52	52	-0.6 (10.3)	-2.3 (7.4)	-5.5 (8.6)
Rps19b	59	67	63	-4.2 (6.9)	-3.8 (6.9)	-4.4 (7.3)
Rps20	52	52	52	-0.6 (7.1)	-3.5 (4.3)	-2.0 (5.4)
Rps24a	36	36	36	0.4 (1.4)	-0.8 (1.6)	-1.2 (1.4)
Rps25a/b	52	52	52	-1.0 (5.0)	-1.1 (6.4)	-1.3 (7.3)
Rps26a	49	42	50	2.3 (5.9)	-1.8 (7.3)	-4.6 (5.1)
Rps28a/b	70	58	64	-2.3 (11.7)	-3.6 (7.6)	-3.4 (5.6)

Supplementary Table S4. Quantification of yeast ribosomal proteins by LC-MS/MS¹.

Frequency of TTG	# of TTG	Protein	Sequence (location of the peptide)	<i>m/z</i> M²⁺ ion
0.68	13	Rpl6a	EANLFPEQQNK (118-128)	659.3198
0.75	15	Rpl6b	EANLFPEQQTK (118-128)	652.8223
0.85	17	Rpl7a	TAEQVAAER (22-30)	487.7433
0.85	17	Rpl7b	TAEQIAAER (22-30)	494.7513
0.50	9	Rpl16a	VASANATAAESDVAK (178-192)	702.8463
0.82	14	Rpl16b	VSSASAAASESDVAK (177-191)	690.3303
1.00	7	Rpl22a	LAFYQVTPEEDEEEDEE (105-121)	1036.4233
0.38	3	Rpl22b	LVFYQVTPEDAEEEDDE (105-121)	1071.9418
0.83	5	Rpl33b	IEGVATPQDAQFYLK (32-47)	868.9408
0.67	4	Rpl33a	IEGVATPQEAQFYLK (32-47)	875.9488
0.67	4	Rpl36a	VTSMTPARK (17-25)	466.2443
1.00	6	Rpl36b	VTQMTPARK (17-25)	486.7573
0.86	18	Rps7a	ILEDLVFPTEIVGK (125-138)	786.9423
0.67	14	Rps7b	VLEDMVFPTTEIVGK (125-138)	788.9128

¹The indicated peptides, which uniquely identify each ribosomal protein in a polysome preparation, were quantified by LC-MS/MS in tryptic digests of purified ribosomal proteins as described in Methods.

²Proportion of leucines encoded by the TTG codon in the yeast ribosomal protein genes

Supplementary Table S5. Relative quantification of ribosomal protein paralogs in untreated and H₂O₂-exposed wild type *S. cerevisiae*. Peptides from trypsinized ribosomal proteins were identified and quantified by LC-MS/MS analysis, as described in Materials and Methods.

	Untreated wild type				H ₂ O ₂ -exposed wild type				P value Unt. vs H ₂ O ₂ ³
	Exp. 1 ¹	Exp. 2	Exp. 3	Mean ± SD	Exp. 1	Exp. 2	Exp. 3	Mean ± SD	
Rpl6A (Low TTG)	37202	34838	32168		29167	35729	36437		
Rpl6B (High TTG)	37772	34787	35296		32688	37779	42100		
Ratio (High:Low)²	1.02	1.00	1.10	1.0 ± 0.05	1.12	1.06	1.16	1.1 ± 0.05	0.15
Rpl7A (High TTG)	52125	58358	63886		74369	82757	83302		
Rpl7B (Low TTG)	17710	19592	17632		23190	27501	25342		
Ratio (High:Low)	2.94	2.98	3.62	3.2 ± 0.4	3.21	3.01	3.29	3.2 ± 0.1	0.96
Rpl16A (Low TTG)	26441	25322	26059		30370	32684	32427		
Rpl16B (High TTG)	47808	48619	45449		61319	65143	64909		
Ratio (High:Low)	1.81	1.92	1.74	1.8 ± 0.09	2.02	1.99	2.00	2.0 ± 0.01	0.03
Rpl22A (High TTG)	82104	78812	79959		100923	113122	104331		
Rpl22B (Low TTG)	5135	4540	4855		5003	5433	4238		
Ratio (High:Low)	15.99	17.36	16.47	17 ± 0.7	20.17	20.82	24.62	22 ± 2.5	0.02
Rpl36A (Low TTG)	19685	21034	20425		24329	25429	23785		
Rpl36B (High TTG)	66330	64554	59024		71843	80215	78331		
Ratio (High:Low)	3.37	3.07	2.89	3.1 ± 0.2	2.95	3.15	3.29	3.1 ± 0.2	0.89
Rpl33A (High TTG)	98668	93021	100545		118034	139000	129200		
Rpl33B (Low TTG)	38656	36228	38861		41246	53358	46685		
Ratio (High:Low)	2.55	2.57	2.59	2.6 ± 0.02	2.86	2.61	2.77	2.7 ± 0.1	0.08
Rps7A (High TTG)	114436	112016	117772		134724	165935	149546		
Rps7B (Low TTG)	33420	33119	32254		38212	46501	40892		
Ratio (High:Low)	3.42	3.38	3.65	3.5 ± 0.1	3.53	3.57	3.66	3.6 ± 0.07	0.35

¹ Data from each of three experiments (Exp.) represent mass spectrometer signal intensities for paralog-derived peptides
² Ratio of the signal intensity for the ribosomal protein paralog with high TTG frequency to that for the low-TTG paralog
³ P-value (Student's t-test) for the comparison of untreated wild type cells to H₂O₂-treated wild type cells

Supplementary Table S6. Relative quantification of ribosomal protein paralogs in untreated *trm4Δ* mutant *S. cerevisiae* and H₂O₂-exposed *trm4* mutant *S. cerevisiae*. Peptides from trypsinized ribosomal proteins were identified and quantified by LC-MS/MS analysis, as described in Materials and Methods.

	Untreated <i>trm4Δ</i> mutant				H ₂ O ₂ -exposed <i>trm4Δ</i> mutant				P value Unt. vs H ₂ O ₂ ³	P value Unt. WT vs <i>trm4Δ</i> ⁴
	Exp. 1 ¹	Exp. 2	Exp. 3	Mean ± SD	Exp. 1	Exp. 2	Exp. 3	Mean ± SD		
Rpl6A (Low TTG)	34839	33189	45467		34448	37473	36774			
Rpl6B (High TTG)	35890	31606	45913		35444	35900	38462			
Ratio (High:Low)²	1.03	0.95	1.01	1.0 ± 0.04	1.03	0.96	1.05	1.0 ± 0.05	0.72	0.36
Rpl7A (High TTG)	62527	54725	68598		57060	44969	48997			
Rpl7B (Low TTG)	16287	12382	22589		12710	15531	14762			
Ratio (High:Low)	3.84	4.42	3.04	3.8 ± 0.7	4.49	2.90	3.32	3.6 ± 0.8	0.77	0.27
Rpl16A (Low TTG)	24239	21581	29295		23720	22763	25216			
Rpl16B (High TTG)	40599	34275	49250		35821	37258	41661			
Ratio (High:Low)	1.67	1.59	1.68	1.6 ± 0.05	1.51	1.64	1.65	1.6 ± 0.08	0.42	0.04
Rpl22A (High TTG)	68494	62884	91551		65753	72045	75433			
Rpl22B (Low TTG)	6567	5868	7976		6229	7390	6490			
Ratio (High:Low)	10.43	10.72	11.48	11 ± 0.5	10.56	9.75	11.62	11 ± 0.9	0.73	0
Rpl36A (Low TTG)	22614	15387	23366		22005	18688	18690			
Rpl36B (High TTG)	56138	51568	68440		49292	52990	58109			
Ratio (High:Low)	2.48	3.35	2.93	2.9 ± 0.4	2.24	2.84	3.11	2.7 ± 0.4	0.62	0.55
Rpl33A (High TTG)	92192	81121	113781		85621	91965	100247			
Rpl33B (Low TTG)	37164	31947	41556		32080	37467	36725			
Ratio (High:Low)	2.48	2.54	2.74	2.6 ± 0.1	2.67	2.45	2.73	2.6 ± 0.1	0.79	0.84
Rps7A (High TTG)	99232	96376	149868		118242	132693	131115			
Rps7B (Low TTG)	30173	26912	45140		36514	38219	38574			
Ratio (High:Low)	3.29	3.58	3.32	3.4 ± 0.2	3.24	3.47	3.40	3.4 ± 0.1	0.83	0.51

¹ Data from each of three experiments (Exp.) represent mass spectrometer signal intensities for paralog-derived peptides
² Ratio of the signal intensity for the ribosomal protein paralog with high TTG frequency to that for the low-TTG paralog
³ P-value (Student's t-test) for the comparison of untreated *trm4Δ* mutant cells to H₂O₂-treated *trm4Δ* mutant cells
⁴ P-value (Student's t-test) for the comparison of untreated wild type cells to untreated *trm4Δ* mutant cells

Supplementary Table S7. Relative mRNA levels of ribosomal protein genes in wild type and *trm4Δ* mutants. As described in Supplementary Methods, real-time quantitative PCR was performed on RNA samples from wild type and *trm4Δ* mutants and the changes in expression for the target genes relative to the reference gene (*ACT1*) (rightmost column) were calculated by the $2^{-\Delta\Delta C_t}$ method². The average threshold cycle number, C_t , for the target gene (*RPL*) and reference gene (*ACT1*) was calculated for three biological replicates. Average $\Delta C_t = (\text{average } C_{tRPL} - \text{average } C_{tACT1})$, with SD calculated by standard error propagation. Average $\Delta\Delta C_t = (\text{average } \Delta C_{t\text{Treatment}} - \text{average } \Delta C_{t\text{WT}})$, with SD calculated by standard error propagation. The value $2^{-\Delta\Delta C_t}$ gives the fold-change of the target gene relative to the reference gene, with values in parentheses representing the average \pm 1SD. The target genes include: (A) *RPL16A*, (B) *RPL16B*, (C) *RPL22A*, and (D) *RPL22B*.

A	RPL16A Mean $C_t \pm$ SD	ACT1 Mean $C_t \pm$ SD	$\Delta C_t \pm$ SD	$\Delta\Delta C_t \pm$ SD	RPL16A fold- change relative to ACT1
Untreated WT	13.03 \pm 0.68	12.99 \pm 0.23	0.04 \pm 0.72	0 \pm 0.72	1 (0.6-1.7)
WT + H ₂ O ₂	13.05 \pm 0.24	13.12 \pm 0.26	-0.08 \pm 0.35	-0.11 \pm 0.35	1.1 (0.8-1.4)
Untreated <i>trm4Δ</i>	12.63 \pm 0.28	13.27 \pm 0.24	-0.64 \pm 0.37	-0.68 \pm 0.37	1.6 (1.2-2.1)
<i>trm4Δ</i> + H ₂ O ₂	12.58 \pm 0.55	13.09 \pm 0.14	-0.51 \pm 0.57	-0.55 \pm 0.57	1.5 (1.0-2.2)

B	RPL16B Average $C_t \pm$ SD	ACT1 Average $C_t \pm$ SD	$\Delta C_t \pm$ SD	$\Delta\Delta C_t \pm$ SD	RPL16B fold- change relative to ACT1
Untreated WT	13.43 \pm 0.60	12.99 \pm 0.23	0.44 \pm 0.64	0 \pm 0.64	1 (0.6-1.6)
WT + H ₂ O ₂	13.36 \pm 0.20	13.12 \pm 0.26	0.23 \pm 0.33	-0.21 \pm 0.33	1.2 (0.9-1.5)
Untreated <i>trm4Δ</i>	13.24 \pm 0.38	13.27 \pm 0.24	-0.02 \pm 0.45	-0.46 \pm 0.45	1.4 (1.0-1.9)
<i>trm4Δ</i> + H ₂ O ₂	12.76 \pm 0.17	13.09 \pm 0.14	-0.33 \pm 0.22	-0.77 \pm 0.14	1.7 (1.4-2.0)

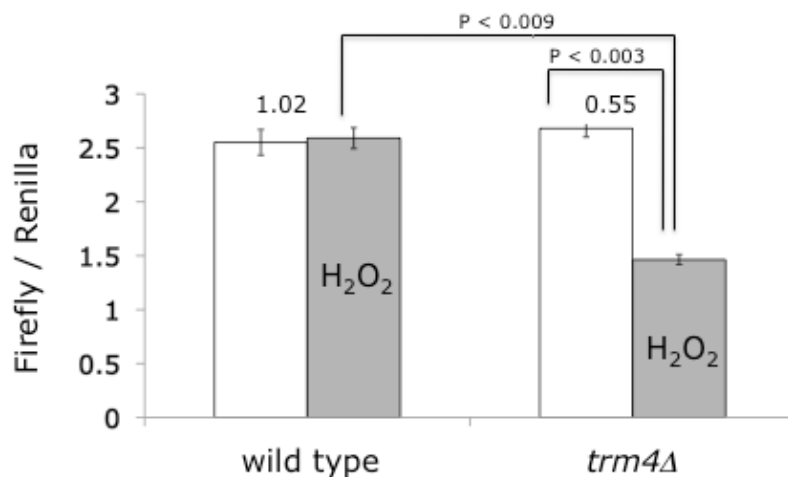
C	RPL22A Average $C_t \pm$ SD	ACT1 Average $C_t \pm$ SD	$\Delta C_t \pm$ SD	$\Delta\Delta C_t \pm$ SD	RPL22A fold- change relative to ACT1
Untreated WT	14.20 \pm 0.26	12.99 \pm 0.23	1.21 \pm 0.35	0 \pm 0.35	1 (0.8-1.3)
WT + H ₂ O ₂	14.57 \pm 0.67	13.12 \pm 0.26	1.44 \pm 0.72	0.24 \pm 0.72	0.8 (0.5-1.4)
Untreated <i>trm4Δ</i>	14.18 \pm 0.11	13.27 \pm 0.24	0.92 \pm 0.27	-0.29 \pm 0.27	1.2 (1-1.5)
<i>trm4Δ</i> + H ₂ O ₂	14.22 \pm 0.65	13.09 \pm 0.14	1.13 \pm 0.67	-0.09 \pm 0.67	1.1 (0.7-1.7)

D	RPL22B Average $C_t \pm$ SD	ACT1 Average $C_t \pm$ SD	$\Delta C_t \pm$ SD	$\Delta\Delta C_t \pm$ SD	RPL22B fold- change relative to ACT1
Untreated WT	16.65 \pm 0.32	12.99 \pm 0.23	3.66 \pm 0.40	0 \pm 0.40	1 (0.8-1.3)
WT + H ₂ O ₂	16.83 \pm 0.16	13.12 \pm 0.26	3.70 \pm 0.30	0.04 \pm 0.30	1 (0.8-1.2)
Untreated <i>trm4Δ</i>	16.54 \pm 0.15	13.27 \pm 0.24	3.28 \pm 0.28	-0.39 \pm 0.28	1.3 (1.1-1.6)
<i>trm4Δ</i> + H ₂ O ₂	16.44 \pm 0.22	13.09 \pm 0.14	3.35 \pm 0.26	-0.31 \pm 0.26	1.2 (1.0-1.5)

Supplementary Table S8: Primer sequences for real-time PCR analysis of ribosomal protein transcripts (see Supplementary Methods for details).

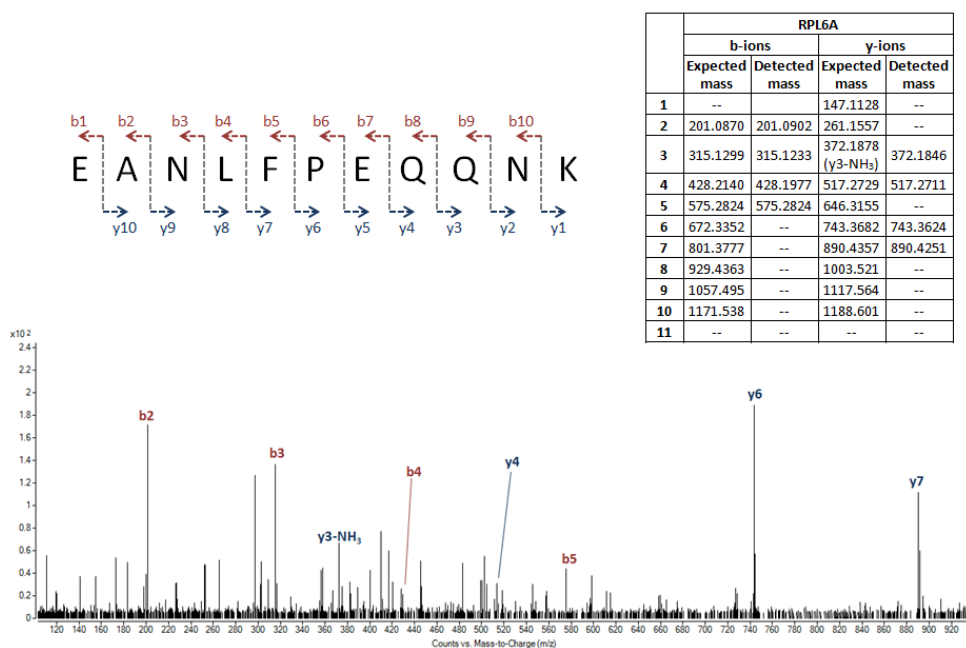
Gene	Forward (5' to 3')	Reverse (5' to 3')
<i>ACT1</i>	GAAAAGATCTGGCATCATACCTTC	AAAACGGCTTGGATGGAAAC
<i>RPL16A</i>	AGGTCGTTTAGCTTCCGTTGTTGCT	GCGGCCTTACCACGAGCAGT
<i>RPL16B</i>	GTTGGGTCGTTTGGCCTCCACTA	GCCTTACCACGGGCGGTCTT
<i>RPL22A</i>	AGATTGCCAAGACCTTTACCGTCGA	CCATCTTCAGTGACAGTGACAGCGT
<i>RPL22B</i>	AAACGGAGTCTTCGATCCGGCTT	GTCAGCATCTTCAGGGGTGACTTGA

Supplementary Figure S2. Control experiment for the study of H₂O₂ and Trm4 methyltransferase control gene expression at the level of TTG codon usage based on a dual Firefly and Renilla luciferase-based reporter system. Wild type and *trm4Δ* mutant yeast cells were transformed with Firefly and Renilla luciferase-based reporters (see Methods), in which the frequency of the TTG codon was varied in the reporter gene (Firefly luciferase) and reporter activity was quantified in H₂O₂-exposed (gray bars) and unexposed cells (white bars). The results presented here are for the unmodified reporters (Renilla and Firefly) containing normal TTG usage (1X). The ratio of treated to untreated is indicated above each condition. Data represent mean ± deviation about the mean for three biological replicates.

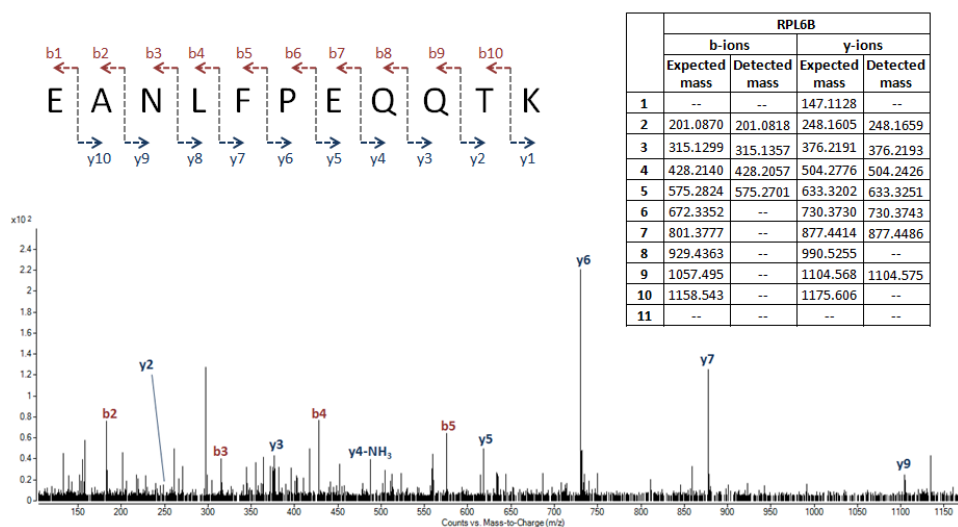


Supplementary Figure S3. Mass spectrometric analysis of ribosomal proteins. As described in the Methods section, tryptic peptides unique to each member of the 7 pairs of ribosomal protein paralogs shown in Supplementary Table S3 were identified by collision-induced dissociation using a QTOF mass spectrometer. The sequence, CID spectrum and expected and detected b- and y-ion mass values for each peptide are shown in the panels below: (A) Rpl6a; (B) Rpl6b; (C) Rpl7a; (D) Rpl7b; (E) Rpl16a; (F) Rpl16b; (G) Rpl22a; (H) Rpl22b; (I) Rpl33a; (J) Rpl33b; (K) Rpl36a; (L) Rpl36b; (M) Rps7a; and (N) Rps7b.

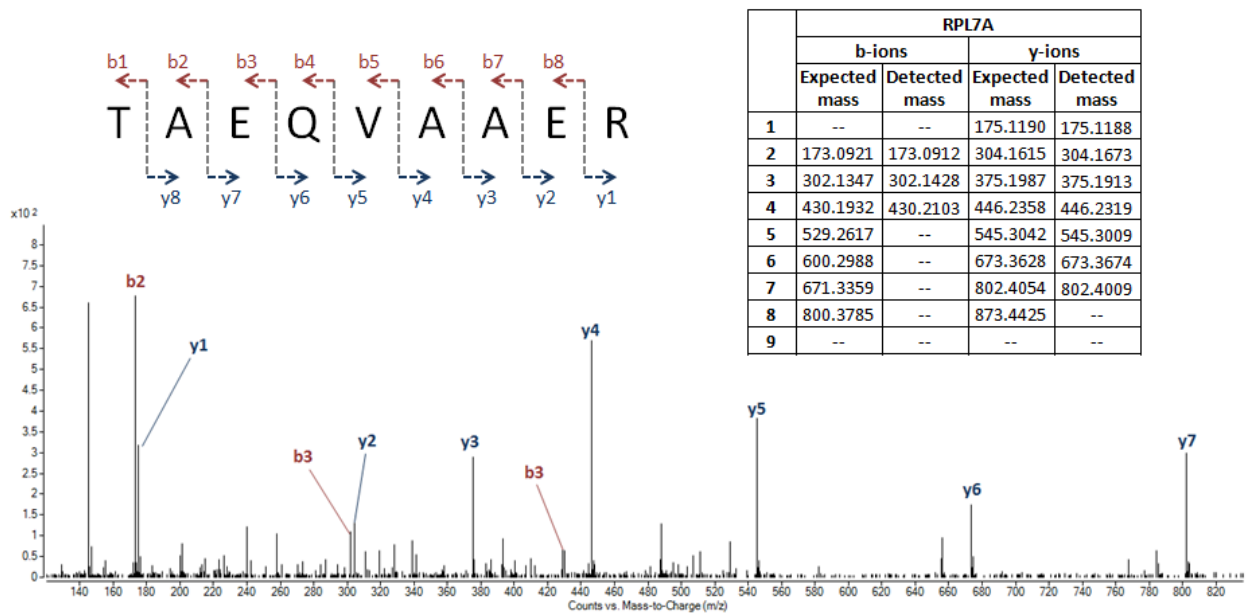
A



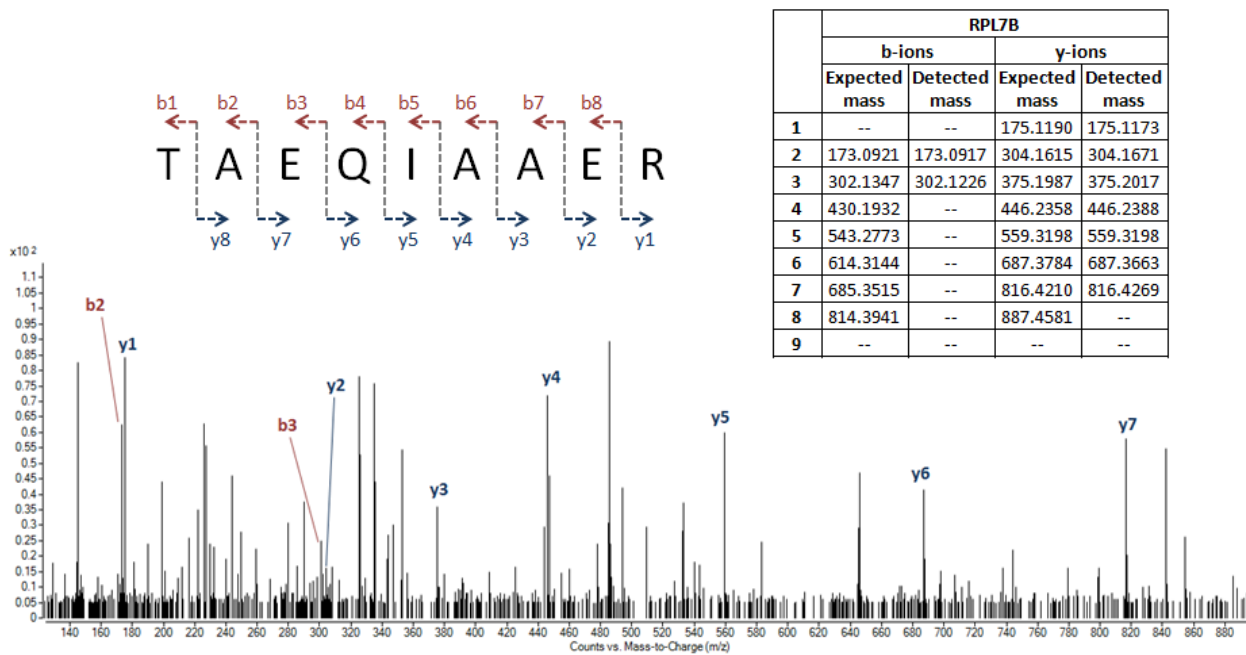
B



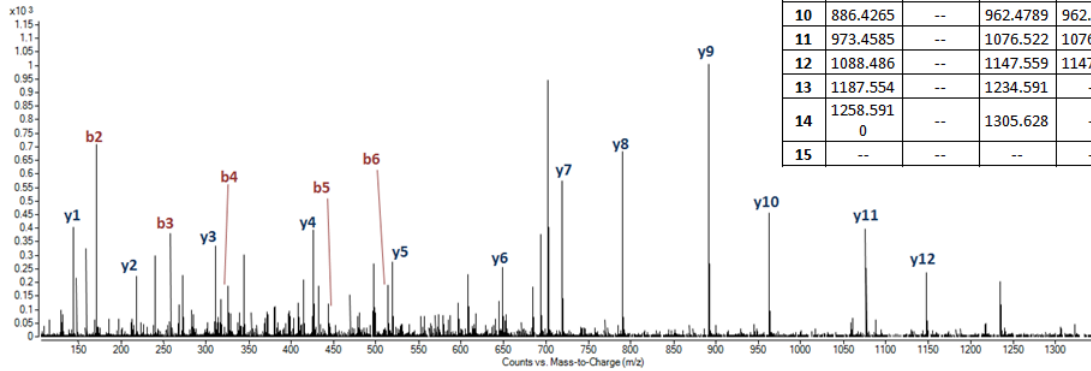
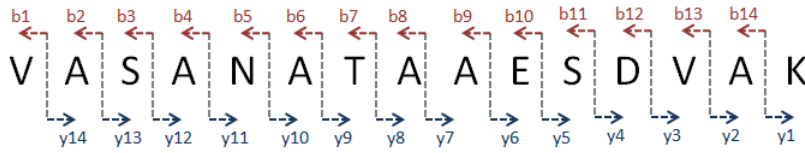
C



D

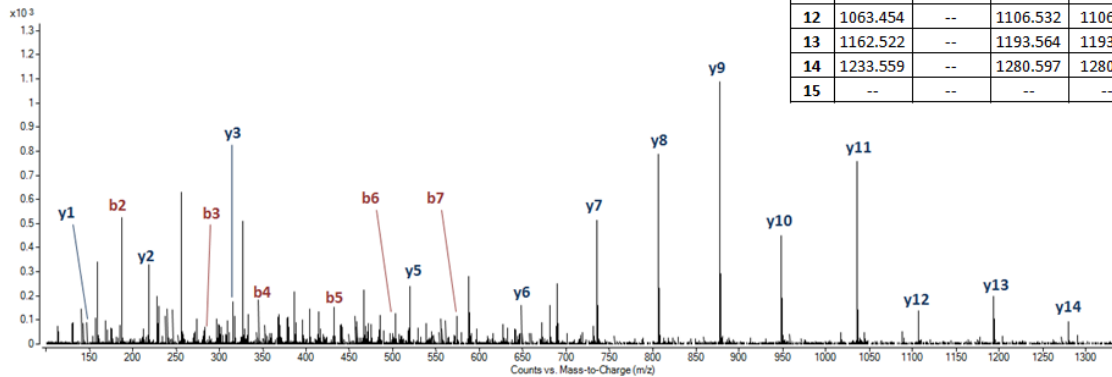
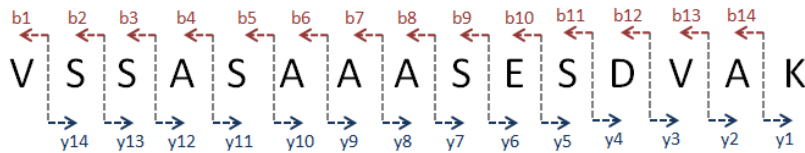


E



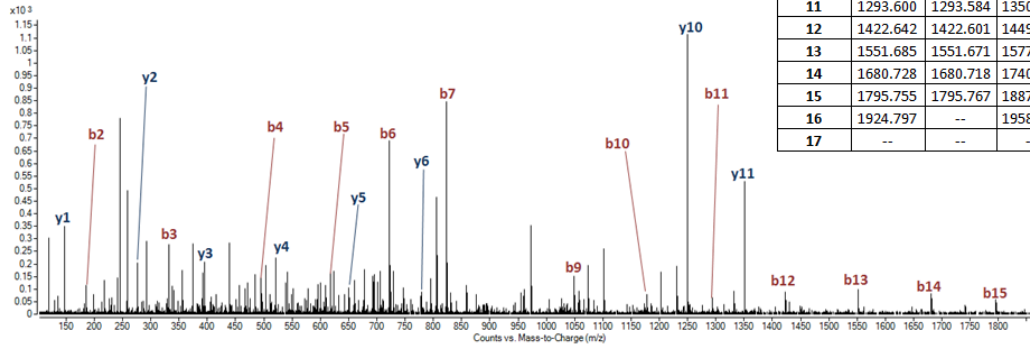
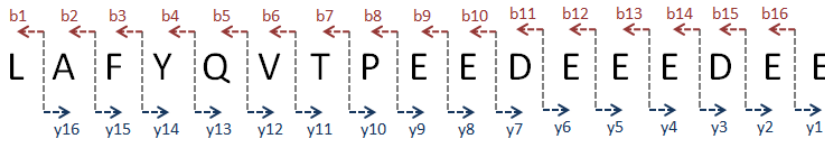
	RPL16A			
	b-ions		y-ions	
	Expected mass	Detected mass	Expected mass	Detected mass
1	--	--	147.1128	147.1103
2	171.1128	171.1102	218.1499	218.1502
3	258.1448	258.1402	317.2183	317.2167
4	329.1819	329.1748	432.2453	432.2375
5	443.2249	443.2135	519.2773	519.2664
6	514.2620	514.2597	648.3199	648.3131
7	615.3097	--	719.3570	719.3486
8	686.3468	--	790.3941	790.3827
9	757.3839	--	891.4418	891.4268
10	886.4265	--	962.4789	962.4716
11	973.4585	--	1076.522	1076.412
12	1088.486	--	1147.559	1147.557
13	1187.554	--	1234.591	--
14	1258.5910	--	1305.628	--
15	--	--	--	--

F



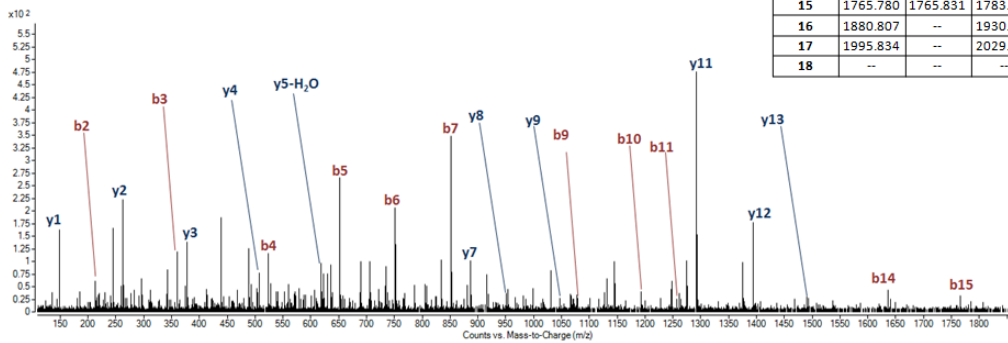
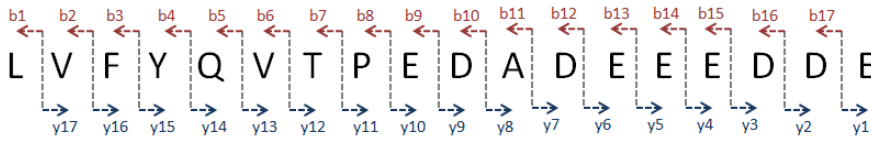
	RPL16B			
	b-ions		y-ions	
	Expected mass	Detected mass	Expected mass	Detected mass
1	--	--	147.1128	147.1074
2	187.1077	187.1054	218.1499	218.1457
3	274.1397	274.1341	317.2183	317.2075
4	345.1769	345.172	432.2453	--
5	432.2089	432.2041	519.2773	519.2682
6	503.2460	503.2423	648.3199	648.3192
7	574.2831	574.2731	735.3519	735.3468
8	645.3202	--	806.3890	806.3727
9	732.3523	--	877.4262	877.4169
10	861.3949	--	948.4633	948.4472
11	948.4269	--	1035.495	1035.476
12	1063.454	--	1106.532	1106.517
13	1162.522	--	1193.564	1193.561
14	1233.559	--	1280.597	1280.629
15	--	--	--	--

G



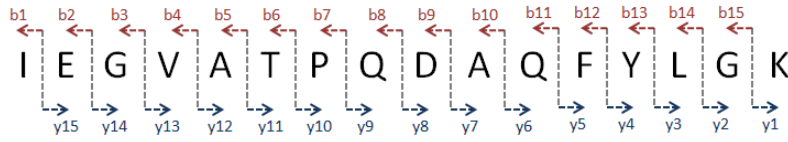
	RPL22A			
	b-ions		y-ions	
	Expected mass	Detected mass	Expected mass	Detected mass
1	--	--	148.0604	148.0576
2	185.1285	185.1251	277.1030	277.0992
3	332.1969	332.1974	392.1300	392.1257
4	495.2602	495.2576	521.1726	521.1600
5	623.3188	623.3119	650.2152	650.2152
6	722.3872	722.3821	779.2577	779.2301
7	823.4349	823.4325	894.2874	--
8	920.4876	--	1023.327	--
9	1049.530	1049.528	1152.370	--
10	1178.573	1178.583	1249.423	1249.415
11	1293.600	1293.584	1350.470	1350.466
12	1422.642	1422.601	1449.539	--
13	1551.685	1551.671	1577.597	--
14	1680.728	1680.718	1740.661	--
15	1795.755	1795.767	1887.729	--
16	1924.797	--	1958.766	--
17	--	--	--	--

H

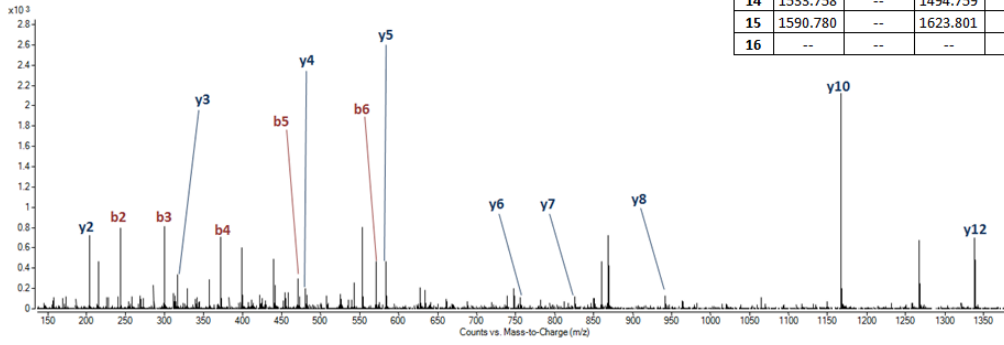


	RPL22B			
	b-ions		y-ions	
	Expected mass	Detected mass	Expected mass	Detected mass
1	--	--	148.0604	148.0661
2	213.1598	213.1677	263.0874	263.0825
3	360.2282	360.2146	378.1143	378.124
4	523.2915	523.2985	507.1569	507.1633
5	651.3501	651.358	618.1889 (y5-H ₂ O)	618.1894
6	750.4185	750.4256	765.2421	--
7	851.4662	851.4692	880.2690	880.2449
8	948.5189	--	951.3062	951.3154
9	1077.562	1077.576	1066.333	1066.341
10	1192.589	1192.59	1195.376	--
11	1263.626	--	1292.429	--
12	1378.653	--	1393.476	--
13	1507.695	--	1492.545	--
14	1636.738	1636.738	1620.603	--
15	1765.780	1765.831	1783.667	--
16	1880.807	--	1930.735	--
17	1995.834	--	2029.803	--
18	--	--	--	--

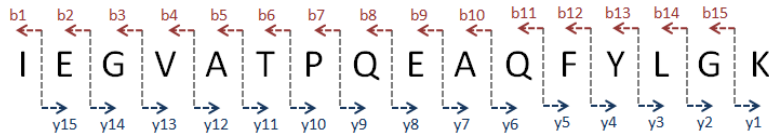
I



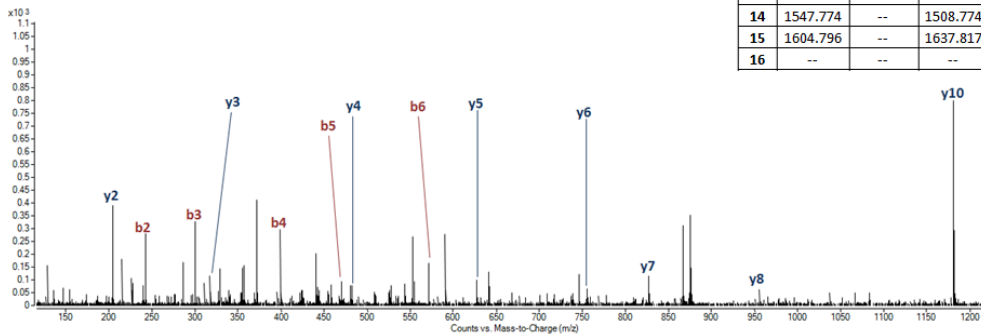
	RPL33A			
	b-ions		y-ions	
	Expected mass	Detected mass	Expected mass	Detected mass
1	--	--	147.1128	--
2	243.1339	243.1356	204.1343	204.1336
3	300.1554	300.1547	317.2183	317.2199
4	399.2238	399.2216	480.2817	480.2965
5	470.2609	470.2603	627.3501	627.3487
6	571.3086	571.3072	755.4087	755.4039
7	668.3614	--	826.4458	826.4454
8	796.4199	--	941.4727	941.4765
9	911.4469	--	1069.531	--
10	982.4840	--	1166.584	1166.585
11	1110.543	--	1267.632	1267.630
12	1257.611	--	1338.669	1338.669
13	1420.674	--	1437.737	--
14	1533.758	--	1494.759	--
15	1590.780	--	1623.801	--
16	--	--	--	--



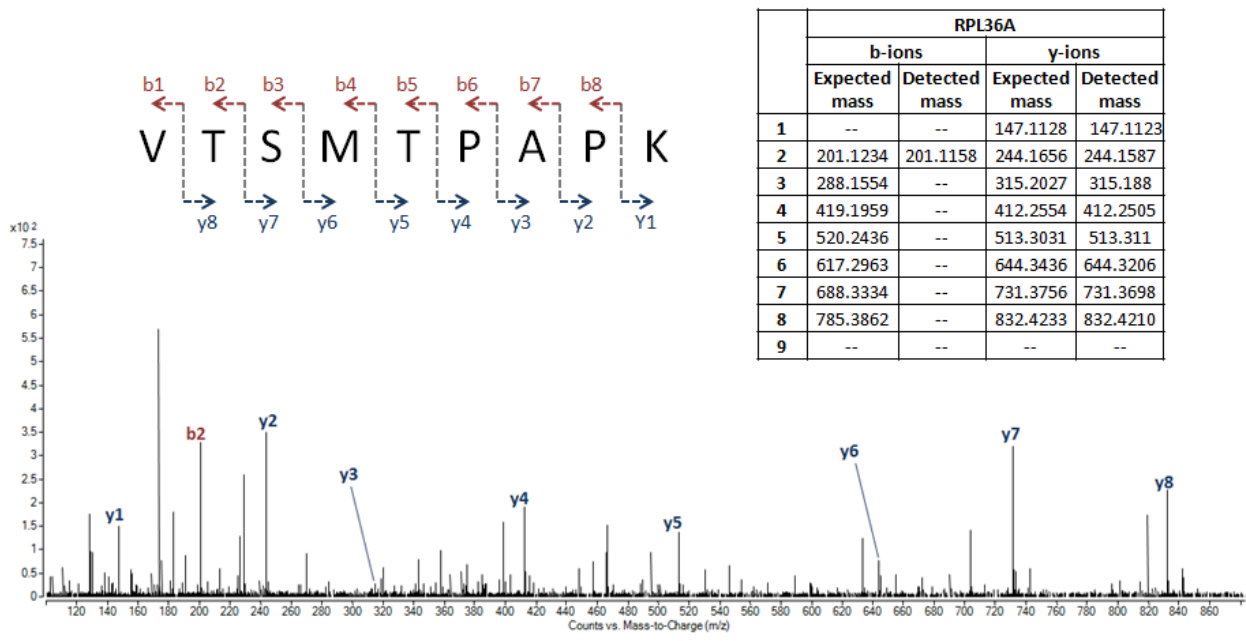
J



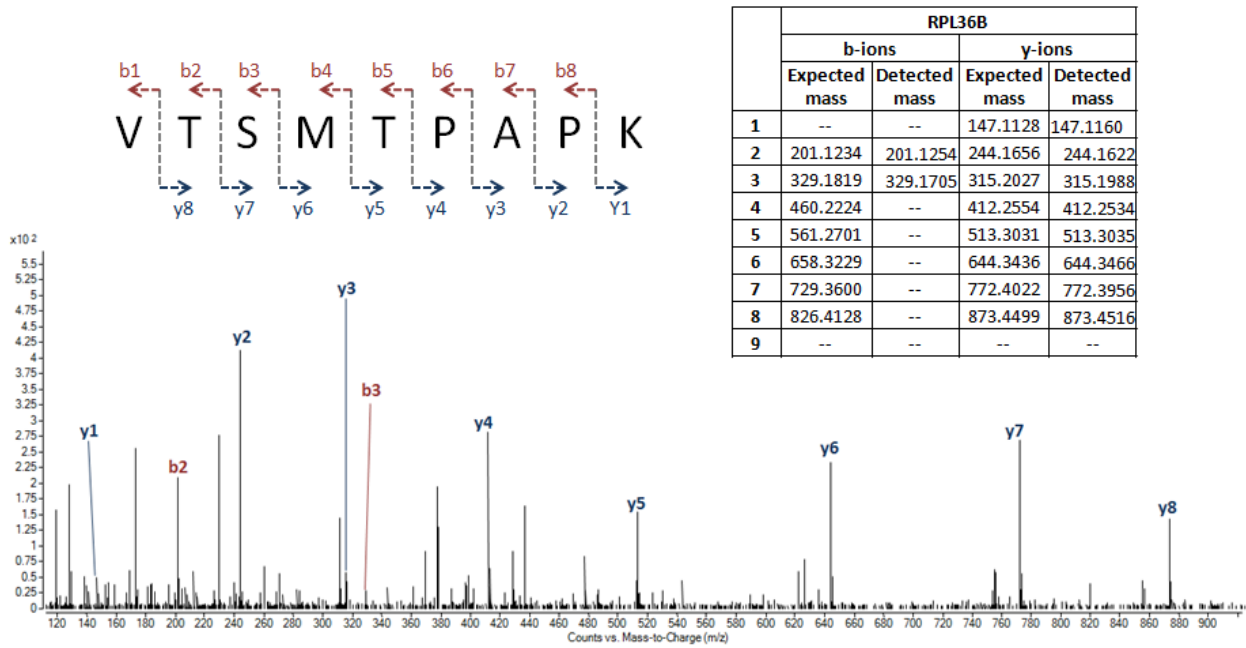
	RPL33B			
	b-ions		y-ions	
	Expected mass	Detected mass	Expected mass	Detected mass
1	--	--	147.1128	--
2	243.1339	243.1369	204.1343	204.1328
3	300.1554	300.1513	317.2183	317.2187
4	399.2238	399.2188	480.2817	480.2843
5	470.2609	470.2501	627.3501	627.3490
6	571.3086	571.3026	755.4087	755.4096
7	668.3614	--	826.4458	826.4491
8	796.4199	--	955.4884	--
9	925.4625	--	1083.547	1083.51
10	996.4997	--	1180.600	1180.597
11	1124.558	--	1281.647	--
12	1271.627	--	1352.685	--
13	1434.690	--	1451.753	--
14	1547.774	--	1508.774	--
15	1604.796	--	1637.817	--
16	--	--	--	--



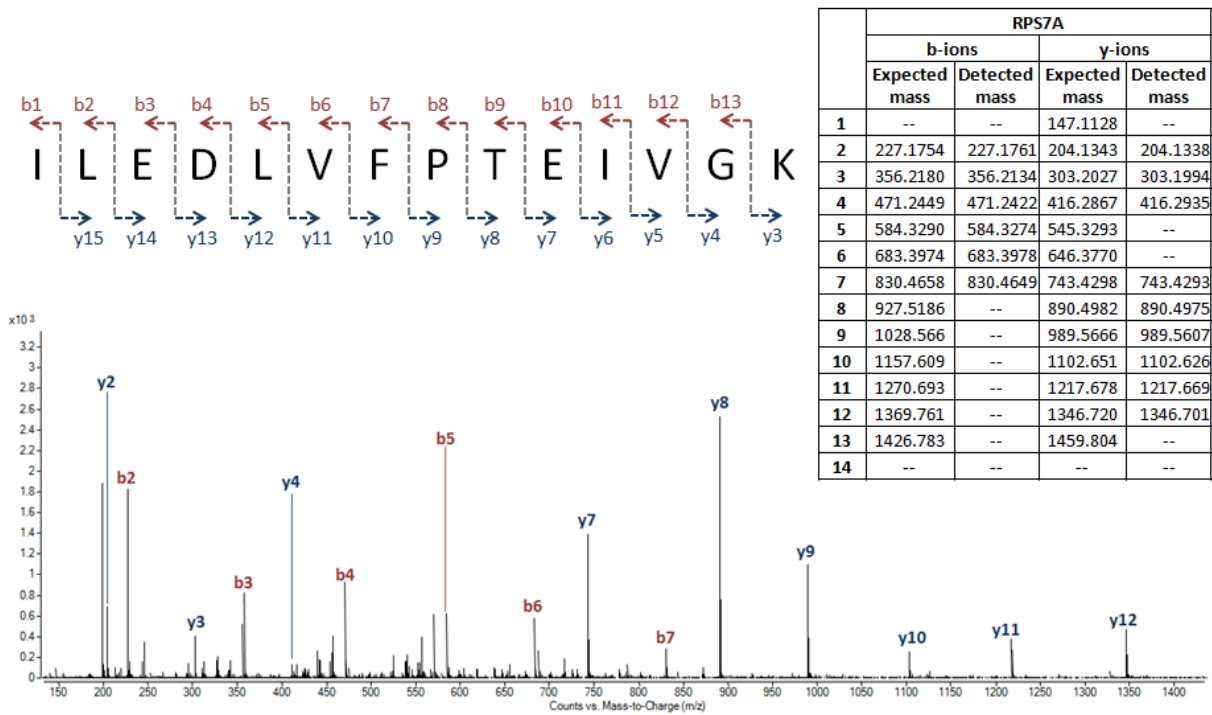
K



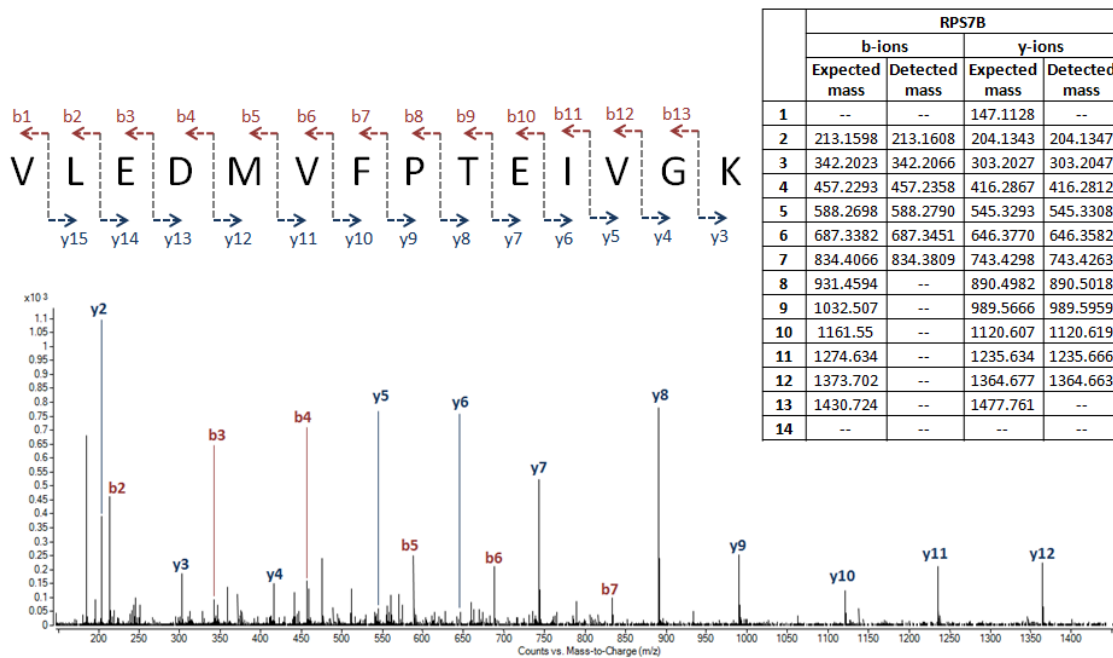
L



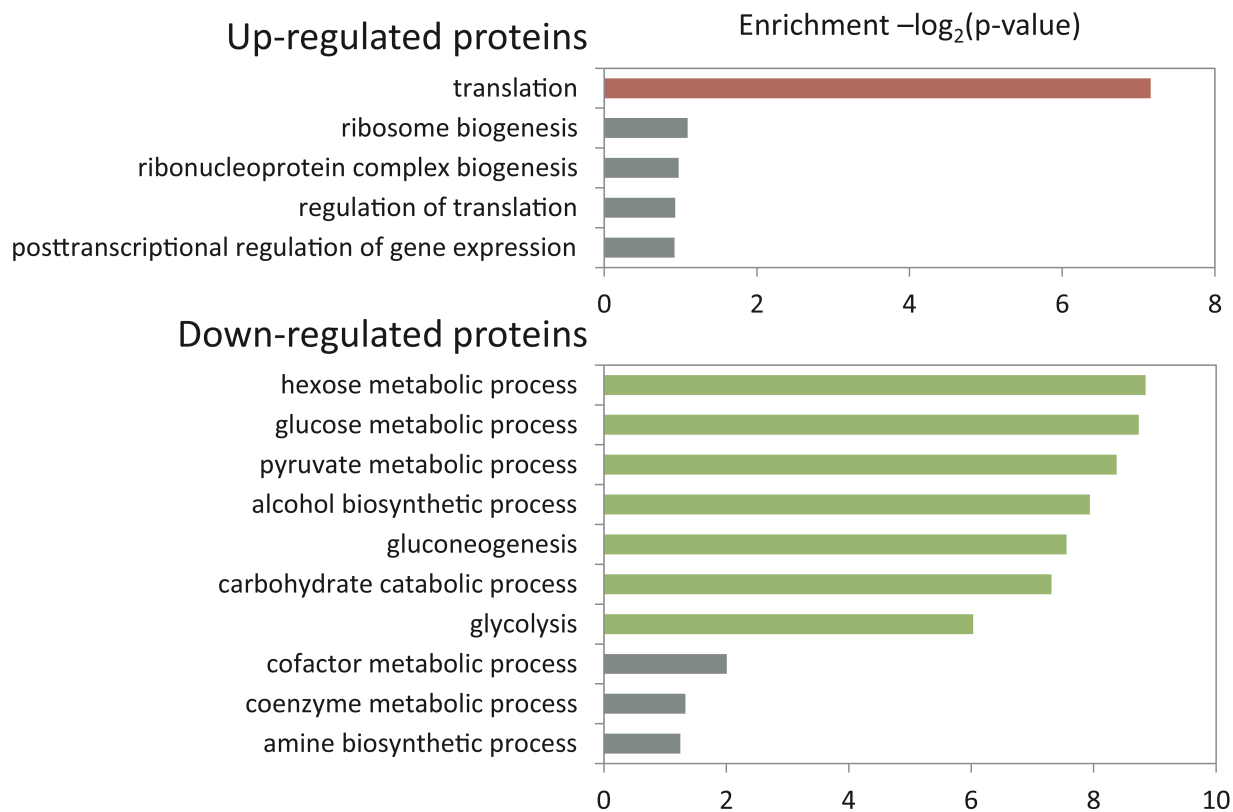
M



N



Supplementary Figure S4: Gene Ontology (GO) analysis of genes up- and down-regulated by H₂O₂ exposure of wild-type yeast.



SUPPLEMENTARY METHODS

Exposure of *S. cerevisiae* to H₂O₂. Mid-log phase cultures of wild-type, *rpl16a*Δ, *rpl16b*Δ, *rpl22a*Δ, and *rpl22b*Δ strains of *S. cerevisiae* BY4741 were exposed to 2 mM hydrogen peroxide (~80% cell survival for wild type) for 1 hr followed by centrifugation at 8000xg for 15 min. The H₂O₂ sensitivity of these strains of yeast was assessed by exposing mid-log phase cultures to 5 mM H₂O₂ (~20% cell survival for wild type) for 1 hr followed by plating a dilution series of each cell type on YPD agar to determine viability.

TRM4 complementation in *trm4* mutant strain. The *TRM4* gene plus 1000 base pairs of upstream DNA, encompassing the promoter, was PCR amplified and inserted in the pRS416 vector using BamH1/Sal1 cloning sites. The resulting pRS416-TRM4 vector was transformed into *trm4*Δ cells and colonies were selected on CSM-URA plates. H₂O₂ viability was performed as described earlier.

Isolation of tRNA. Following exposure to 2 mM H₂O₂, total RNA was isolated from 2 L of mid-log phase BY4741 *S. cerevisiae* cultures. Crude RNA was isolated using TRIzol (Invitrogen, Carlsbad, CA) and ruptured by 5 cycles of bead beating (FastPrep FP120, MP Biomedicals, Solon, OH) for 30 s on setting 5. The extracted crude RNA products were purified by electrophoresis on a 10% polyacrylamide gel containing 8 M urea, with the band corresponding to tRNA visualized by UV-shadowing. The excised gel was crushed and tRNA was recovered by electroelution (Electro-Eluter, Bio-Rad, Hercules, CA).

Purification of tRNA^{Leu(CAA)}. An oligo-based pull-down approach was used to purify tRNA^{Leu(CAA)} from a crude sample of tRNA⁴⁸. With complementarity to the 3' acceptor stem of the tRNA^{Leu(CAA)}, the biotinylated oligodeoxynucleotide for tRNA capture (18 nmol; IDT, Coralville, IA) was bound to NeutrAvidin agarose beads (~0.2 mL; Thermo Scientific, Waltham, MA). tRNA^{Leu(CAA)} isolated from 9 mg of *S. cerevisiae* total tRNA was bound to the oligodeoxynucleotide in 6 X NHE containing 1.2 M NaCl, 30 mM HEPES-KOH, pH 7.5, and 15 mM EDTA at 72 °C for 30 min followed by a slow cool to room temperature for 80 min. The beads-bound complexes were then washed three times with each of 3 X NHE, 1 X NHE and 0.1 X NHE until the UV absorbance (260 nm) fell below 0.01. The target tRNA^{Leu(CAA)} was eluted from the beads with three incubations in 0.1 X NHE at 65 °C for 5 min.

Transcriptional analysis. Total RNA was isolated from *S. cerevisiae* BY4741 using the Qiagen RNeasy Mini kit. An amount of 100 ng of total RNA was used to perform real-time quantitative PCR with an Applied Biosystems Power SYBR Green RNA-to-C_T kit and an Applied Biosystems 7900HT Fast Real-Time PCR System to determine the relative transcription levels of ribosomal protein genes *RPL16A*, *RPL116B*, *RPL22A*, and *RPL22B* with *ACT1* chosen as a housekeeping gene for normalization. Primer sequences are listed in Supplementary Table S8. The ΔΔC_T method was used to compare the transcription levels in different samples⁴⁹.

References for Supplementary Information

- 48 Suzuki, T. Chaplet column chromatography: isolation of a large set of individual RNAs in a single step. *Methods Enzymol* **425**, 231-239 (2007).
- 49 Livak, K. J. & Schmittgen, T. D. Analysis of relative gene expression data using real-time quantitative PCR and the 2(-Delta Delta C(T)) Method. *Methods* **25**, 402-408 (2001).

SUPPLEMENTARY DATA 1

Reprogramming of tRNA modifications controls the oxidative stress response by codon-biased translation of proteins

Clement T.Y. Chan, Yan Ling Joy Pang, Wenjun Deng, I. Ramesh Babu, Madhu
Dyavaiah, Thomas J. Begley and Peter C. Dedon

A summary of identified proteins and their expression levels from a SILAC-based LC-MS/MS proteomic analysis of wild-type and *trm4Δ* yeast exposed to H₂O₂. See Methods for experimental details.

Access number	Gene symbol	Protein name	TTG frequency	Trm4-Wild		H2O2-treated WT		H2O2-treated trm4Δ	
				Protein ratio (trm4Δ/WT)	p-value	Protein ratio (treated/untreated)	p-value	Protein ratio (Treated/untreated)	p-value
O13516	RPS9A	40S ribosomal protein S9-A	60.00%	1.04	0.47	0.93	0.28	1.13	5.93E-03
P00330	ADH1	Alcohol dehydrogenase 1	79.17%	0.83	7.46E-03	0.96	0.26	0.99	0.83
P00331	ADH2	Alcohol dehydrogenase 2	60.00%	0.94	0.18	0.76	2.31E-03	0.81	9.82E-04
P00358	TDH2	Glyceraldehyde-3-phosphate dehydrogenase 2	95.24%	0.85	9.42E-04	0.88	8.84E-04	0.94	0.11
P00359	TDH3	Glyceraldehyde-3-phosphate dehydrogenase 3	95.24%	0.78	6.65E-05	0.91	0.03	1.02	0.48
P00498	HIS1	ATP phosphoribosyltransferase	30.00%	0.90	0.17	0.82	0.08	1.00	0.97
P00549	CDC19	Pyruvate kinase 1	91.43%	0.92	0.12	0.90	0.01	0.96	0.38
P00560	PGK1	Phosphoglycerate kinase	87.80%	0.69	4.63E-06	0.74	5.63E-04	1.06	0.08
P00815	HIS4	Histidine biosynthesis trifunctional protein	36.59%	1.03	0.89	NA	NA	0.87	0.48
P00817	IPP1	Inorganic pyrophosphatase	64.71%	0.77	2.44E-04	0.80	0.01	0.93	0.25
P00830	ATP2	ATP synthase subunit beta, mitochondrial	47.92%	1.27	0.57	1.04	0.92	1.52	0.31
P00890	CIT1	Citrate synthase, mitochondrial	33.33%	1.10	0.06	0.55	1.45E-05	0.87	0.22
P00924	ENO1	Enolase 1	90.00%	0.79	6.06E-03	0.80	0.01	0.96	0.54
P00925	ENO2	Enolase 2	92.11%	0.76	1.11E-05	1.13	0.01	1.00	0.80
P00942	TPI1	Triosephosphate isomerase	78.95%	0.75	8.13E-03	0.87	0.03	1.04	0.70
P00950	GPM1	Phosphoglycerate mutase 1	82.14%	0.72	1.59E-05	0.90	6.60E-03	1.04	0.24
P02294	HTB2	Histone H2B.2	83.33%	0.82	6.39E-03	0.76	1.25E-03	1.05	0.37
P02365	RPS6A	40S ribosomal protein S6	95.00%	0.92	0.39	0.99	0.86	1.19	0.11
P02400	RPP2B	60S acidic ribosomal protein P2-beta	55.56%	1.03	0.40	1.01	0.88	1.11	0.01
P02406	RPL28	60S ribosomal protein L28	100.00%	0.99	0.96	1.18	0.12	0.92	0.52
P02994	TEF1	Elongation factor 1-alpha	87.50%	1.25	4.24E-04	1.08	0.02	1.08	0.12
P03962	URA3	Orotidine 5'-phosphate decarboxylase	38.46%	NA	NA	0.35	0.13	NA	NA
P03965	CPA2	Carbamoyl-phosphate synthase arginine-specific large chain	37.25%	1.73	5.47E-03	1.24	0.16	1.52	8.81E-04
P04451	RPL23A	60S ribosomal protein L23	55.56%	1.16	0.02	0.75	8.97E-05	0.91	0.14
P04456	RPL25	60S ribosomal protein L25	81.82%	1.00	0.92	0.95	0.28	1.00	0.98
P04806	HXK1	Hexokinase-1	60.42%	NA	NA	NA	NA	0.72	7.87E-03
P04807	HXK2	Hexokinase-2	71.43%	1.09	0.91	1.38	0.60	2.59	0.12
P04840	POR1	Mitochondrial outer membrane protein porin 1	58.06%	1.39	2.25E-03	0.90	0.10	1.14	0.12
P05030	PMA1	Plasma membrane ATPase 1	72.09%	1.02	0.74	1.20	0.01	1.07	0.48
P05317	RPP0	60S acidic ribosomal protein P0	84.00%	1.03	0.64	1.06	0.30	1.03	0.27
P05318	RPP1A	60S acidic ribosomal protein P1-alpha	81.82%	1.01	0.95	0.88	0.09	0.89	0.42
P05319	RPP2A	60S acidic ribosomal protein P2-alpha	50.00%	0.96	0.37	1.02	0.58	1.06	0.16
P05694	MET6	5-methyltetrahydropteroyltriglutamate--homocysteine methyltransferase	66.67%	0.31	3.72E-08	0.38	1.31E-06	1.07	0.19
P05735	RPL19A	60S ribosomal protein L19	56.25%	1.11	0.02	1.02	0.61	0.90	0.08
P05736	RPL2A	60S ribosomal protein L2	81.25%	1.07	0.51	1.35	0.02	1.20	0.13
P05738	RPL9A	60S ribosomal protein L9-A	90.00%	0.95	0.10	1.00	0.90	1.01	0.87
P05739	RPL6B	60S ribosomal protein L6-B	75.00%	0.91	0.14	1.07	0.26	1.06	0.39
P05749	RPL22A	60S ribosomal protein L22-A	100.00%	0.91	0.02	0.98	0.73	1.05	0.22
P05750	RPS3	40S ribosomal protein S3	63.16%	1.00	0.87	1.10	5.25E-03	1.03	0.31
P05753	RPS4A	40S ribosomal protein S4	64.00%	0.95	0.52	1.94	0.05	1.09	0.14
P05754	RPS8A	40S ribosomal protein S8	50.00%	1.24	0.03	1.19	0.11	1.08	0.28
P05755	RPS9B	40S ribosomal protein S9-B	90.00%	0.82	1.51E-03	0.93	0.07	1.07	0.22

P05756	RPS13	40S ribosomal protein S13	92.86%	1.10	0.09	1.15	5.09E-03	1.01	0.77
P05759	RPS31	Ubiquitin-40S ribosomal protein S31	78.57%	1.04	0.33	1.13	5.91E-03	1.05	0.32
P06105	SCP160	Protein SCP160	42.86%	NA	NA	NA	NA	0.95	0.78
P06168	ILV5	Ketol-acid reductoisomerase, mitochondrial	85.29%	0.89	1.77E-03	1.02	0.58	1.04	0.19
P06169	PDC1	Pyruvate decarboxylase isozyme 1	90.74%	0.97	0.31	1.20	0.06	1.08	0.08
P06208	LEU4	2-isopropylmalate synthase	41.46%	1.31	0.02	0.94	0.47	2.06	0.48
P06634	DED1	ATP-dependent RNA helicase DED1	56.82%	1.20	5.51E-03	1.41	5.07E-04	0.97	0.63
P07149	FAS1	Fatty acid synthase subunit beta	45.81%	0.45	0.03	0.77	0.36	1.36	0.13
P07251	ATP1	ATP synthase subunit alpha, mitochondrial	67.69%	1.25	0.03	0.76	0.12	0.99	0.59
P07260	CDC33	Eukaryotic translation initiation factor 4E	25.00%	0.99	0.60	1.06	0.33	1.10	0.01
P07262	GDH1	NADP-specific glutamate dehydrogenase 1	64.29%	0.22	0.06	0.71	0.50	NA	NA
P07263	HTS1	Histidyl-tRNA synthetase, mitochondrial	40.91%	0.90	0.48	0.96	0.76	0.97	0.73
P07279	RPL18A	60S ribosomal protein L18	73.33%	0.94	0.43	1.09	0.13	1.12	0.17
P07281	RPS19B	40S ribosomal protein S19-B	87.50%	1.09	0.34	1.23	0.04	1.14	0.02
P07806	VAS1	Valyl-tRNA synthetase, mitochondrial	43.75%	1.00	1.00	1.39	0.45	1.42	0.31
P08018	PBS2	MAP kinase kinase PBS2	22.81%	0.82	0.34	NA	NA	NA	NA
P08524	ERG20	Farnesyl pyrophosphate synthase	62.16%	0.78	0.02	NA	NA	NA	NA
P08566	ARO1	Pentafunctional AROM polypeptide	30.14%	NA	NA	NA	NA	3.86	0.58
P09938	RNR2	Ribonucleoside-diphosphate reductase small chain 1	66.67%	NA	NA	NA	NA	0.93	0.51
POCOW1	RPS22A	40S ribosomal protein S22-A	80.00%	1.07	0.15	1.24	5.99E-03	1.00	0.97
POC2H6	RPL27A	60S ribosomal protein L27-A	71.43%	0.97	0.48	0.98	0.51	1.05	0.19
POC2H8	RPL31A	60S ribosomal protein L31-A	54.55%	1.07	0.17	1.13	0.02	1.06	0.30
P10081	TIF1	ATP-dependent RNA helicase eIF4A	71.43%	0.97	0.58	1.27	0.14	1.05	0.43
P10591	SSA1	Heat shock protein SSA1	89.58%	0.73	2.48E-03	0.93	0.93	0.73	0.02
P10592	SSA2	Heat shock protein SSA2	87.50%	0.76	5.46E-03	1.40	0.06	1.13	0.09
P11075	SEC7	Protein transport protein SEC7	26.37%	NA	NA	NA	NA	0.10	0.33
P11076	ARF1	ADP-ribosylation factor 1	63.16%	NA	NA	1.35	0.02	NA	NA
P11154	PYC1	Pyruvate carboxylase 1	39.42%	NA	NA	NA	NA	1.37	0.04
P11484	SSB1	Heat shock protein SSB1	88.24%	1.02	0.50	1.12	0.01	1.08	0.05
P11745	RNA1	Ran GTPase-activating protein 1	39.06%	1.00	0.97	1.59	0.08	1.20	0.09
P12398	SSC1	Heat shock protein SSC1, mitochondrial	63.27%	0.69	0.02	0.78	0.03	1.20	0.12
P12695	LAT1	Dihydrolipoylysine-residue acetyltransferase component	47.06%	1.47	0.23	0.87	0.05	NA	NA
P12709	PGI1	Glucose-6-phosphate isomerase	87.23%	0.88	2.71E-03	0.86	2.40E-05	0.95	0.33
P13586	PMR1	Calcium-transporting ATPase 1	23.81%	1.30	0.50	NA	NA	0.62	0.28
P13663	HOM2	Aspartate-semialdehyde dehydrogenase	58.82%	1.03	0.93	1.01	0.96	0.99	0.95
P14126	RPL3	60S ribosomal protein L3	85.71%	0.78	0.27	0.92	0.02	1.31	0.24
P14127	RPS17B	40S ribosomal protein S17-B	86.67%	0.83	5.94E-03	0.95	0.04	1.04	0.47
P14540	FBA1	Fructose-bisphosphate aldolase	70.83%	0.93	0.20	0.78	0.03	0.89	0.05
P14742	GFA1	Glucosamine--fructose-6-phosphate aminotransferase [iso	25.00%	0.77	0.33	NA	NA	NA	NA
P15108	HSC82	ATP-dependent molecular chaperone HSC82	67.65%	0.95	0.25	1.15	3.92E-03	1.11	0.03
P15180	KRS1	Lysyl-tRNA synthetase, cytoplasmic	51.92%	1.29	2.14E-04	1.02	0.67	1.00	0.95
P16120	THR4	Threonine synthase	34.78%	1.07	0.18	0.55	0.24	0.75	0.33
P16140	VMA2	V-type proton ATPase subunit B	73.81%	0.86	0.01	0.97	0.43	0.94	0.25
P16467	PDC5	Pyruvate decarboxylase isozyme 2	81.82%	0.91	0.01	0.90	8.57E-03	0.94	0.20
P16474	KAR2	78 kDa glucose-regulated protein homolog	41.94%	0.74	1.81E-03	1.05	0.53	1.09	9.44E-03
P16521	YEF3	Elongation factor 3A	77.01%	1.39	7.39E-04	1.41	1.43E-03	1.17	0.03
P16861	PFK1	6-phosphofructokinase subunit alpha	40.70%	1.04	0.76	1.00	0.94	1.05	0.75

P16862	PFK2	6-phosphofructokinase subunit beta	58.44%	1.01	0.81	1.07	0.39	0.94	0.20
P17076	RPL8A	60S ribosomal protein L8-A	95.00%	1.24	0.03	1.22	0.04	0.95	0.46
P17079	RPL12A	60S ribosomal protein L12	54.55%	1.44	9.64E-03	1.23	3.93E-04	1.03	0.85
P17255	VMA1	V-type proton ATPase catalytic subunit A	47.13%	0.87	0.10	1.02	0.76	0.99	0.90
P17555	SRV2	Adenylyl cyclase-associated protein	41.67%	0.86	0.06	0.79	2.83E-03	0.92	0.36
P17967	PDI1	Protein disulfide-isomerase	56.52%	0.71	8.13E-03	0.93	0.19	0.86	0.39
P18238	AAC3	ADP,ATP carrier protein 3	37.93%	NA	NA	NA	NA	1.99	0.55
P18239	PET9	ADP,ATP carrier protein 2	55.88%	1.49	4.29E-04	0.78	0.07	0.89	0.14
P19097	FAS2	Fatty acid synthase subunit alpha	54.78%	0.70	0.08	1.00	0.99	1.42	0.08
P19358	SAM2	S-adenosylmethionine synthase 2	41.38%	0.28	3.53E-07	0.37	5.06E-06	1.00	0.99
P19657	PMA2	Plasma membrane ATPase 2	46.07%	0.98	0.77	0.97	0.57	1.02	0.79
P19882	HSP60	Heat shock protein 60, mitochondrial	57.14%	0.88	0.69	0.65	0.11	0.88	0.58
P20606	SAR1	Small COPII coat GTPase SAR1	30.77%	1.06	0.77	1.34	0.13	1.06	0.62
P21242	PRE10	Proteasome component C1	23.81%	NA	NA	NA	NA	1.07	0.31
P21372	PRP5	Pre-mRNA-processing ATP-dependent RNA helicase PRP5	20.51%	NA	NA	NA	NA	0.53	0.78
P21592	COX10	Protoheme IX farnesyltransferase, mitochondrial	21.74%	NA	NA	NA	NA	1.07	0.35
P21951	POL2	DNA polymerase epsilon catalytic subunit A	22.12%	2.10	0.63	2.72	0.24	0.25	0.37
P21954	IDP1	Isocitrate dehydrogenase [NADP], mitochondrial	45.95%	1.08	0.19	0.70	4.71E-04	0.94	0.28
P22217	TRX1	Thioredoxin-1	50.00%	0.93	0.72	0.79	0.12	1.36	0.04
P22768	ARG1	Argininosuccinate synthase	64.86%	1.03	0.48	0.65	7.84E-04	0.59	8.32E-05
P23254	TKL1	Transketolase 1	58.73%	1.07	0.28	0.99	0.85	0.97	0.67
P23301	HYP2	Eukaryotic translation initiation factor 5A-1	100.00%	NA	NA	NA	NA	1.13	0.16
P25379	CHA1	Catabolic L-serine/threonine dehydratase	34.78%	0.91	0.57	0.97	0.83	NA	NA
P25443	RPS2	40S ribosomal protein S2	90.48%	1.11	0.33	1.32	0.03	0.99	0.84
P25694	CDC48	Cell division control protein 48	39.13%	0.81	0.03	0.74	0.08	0.88	0.10
P26321	RPL5	60S ribosomal protein L5	73.91%	0.92	0.10	0.96	0.40	1.04	0.51
P26637	CDC60	Leucyl-tRNA synthetase, cytoplasmic	38.96%	1.21	0.02	1.18	0.16	1.04	0.41
P26781	RPS11A	40S ribosomal protein S11	60.00%	1.02	0.66	1.12	9.95E-03	0.98	0.78
P26783	RPS5	40S ribosomal protein S5	92.86%	0.83	0.11	0.95	0.74	1.07	0.59
P26784	RPL16A	60S ribosomal protein L16-A	50.00%	1.25	0.36	1.16	0.03	0.83	0.34
P26785	RPL16B	60S ribosomal protein L16-B	82.35%	1.15	0.16	1.20	0.02	0.96	0.71
P26786	RPS7A	40S ribosomal protein S7-A	85.71%	1.04	0.76	1.23	2.32E-03	0.93	0.59
P27692	SPT5	Transcription elongation factor SPT5	22.22%	0.61	7.11E-04	1.21	0.17	1.30	0.06
P27705	MIG1	Regulatory protein MIG1	31.91%	NA	NA	NA	NA	0.42	0.33
P28272	URA1	Dihydroorotate dehydrogenase (fumarate)	37.93%	NA	NA	NA	NA	0.40	4.61E-06
P29453	RPL8B	60S ribosomal protein L8-B	90.48%	1.09	0.02	NA	NA	1.07	0.06
P29547	CAM1	Elongation factor 1-gamma 1	50.00%	1.09	0.23	1.22	0.11	1.14	0.09
P30952	MLS1	Malate synthase 1, glyoxysomal	45.45%	NA	NA	NA	NA	1.97	0.23
P31116	HOM6	Homoserine dehydrogenase	62.50%	0.68	1.04E-03	0.84	0.01	1.01	0.93
P31373	CYS3	Cystathionine gamma-lyase	57.50%	1.16	0.66	0.48	0.05	0.16	0.20
P32074	SEC21	Coatomer subunit gamma	35.14%	1.00	0.97	3.37	0.40	1.00	0.89
P32324	EFT1	Elongation factor 2	78.26%	1.08	0.34	1.06	0.39	1.03	0.59
P32451	BIO2	Biotin synthase, mitochondrial	34.38%	0.87	0.27	NA	NA	1.68	0.02
P32589	SSE1	Heat shock protein homolog SSE1	50.00%	0.90	0.17	1.18	0.01	1.05	0.53
P32792	YSC83	UPF0744 protein YSC83	23.26%	NA	NA	NA	NA	0.57	0.01
P32827	RPS23A	40S ribosomal protein S23	76.92%	1.01	0.87	1.41	2.04E-04	1.33	1.63E-03
P32855	SEC8	Exocyst complex component SEC8	23.88%	NA	NA	NA	NA	1.09	0.65

P32873	BEM3	GTPase-activating protein BEM3	31.30%	0.91	0.05	1.04	0.34	0.97	0.51
P33299	RPT1	26S protease regulatory subunit 7 homolog	11.43%	0.80	0.74	NA	NA	NA	NA
P33322	CBF5	H/ACA ribonucleoprotein complex subunit 4	40.91%	NA	NA	NA	NA	1.96	0.46
P33334	PRP8	Pre-mRNA-splicing factor 8	19.58%	NA	NA	0.52	0.08	NA	NA
P33401	PGM1	Phosphoglucomutase-1	21.74%	2.49	0.22	0.75	5.12E-03	0.38	0.39
P33442	RPS1A	40S ribosomal protein S1-A	72.73%	0.92	0.08	0.94	0.10	0.98	0.73
P34730	BMH2	Protein BMH2	33.33%	0.89	0.04	0.90	0.03	1.15	0.03
P34760	TSA1	Peroxiredoxin TSA1	82.35%	0.94	0.49	1.01	0.94	1.15	0.12
P35178	RRP1	Ribosomal RNA-processing protein 1	29.03%	1.45	0.59	0.74	0.81	0.44	0.04
P35271	RPS18A	40S ribosomal protein S18	73.33%	1.03	0.36	1.03	0.24	1.06	0.06
P35691	TMA19	Translationally-controlled tumor protein homolog	71.43%	NA	NA	1.54	1.07E-03	NA	NA
P36008	TEF4	Elongation factor 1-gamma 2	54.05%	1.15	0.34	1.51	1.36E-03	1.13	0.33
P36049	EBP2	rRNA-processing protein EBP2	50.00%	6.83	7.78E-09	1.43	0.40	1.22	0.39
P36166	PXL1	Paxillin-like protein 1	13.64%	NA	NA	NA	NA	0.61	0.14
P37012	PGM2	Phosphoglucomutase-2	31.58%	0.96	0.94	0.77	0.10	NA	NA
P38011	ASC1	Guanine nucleotide-binding protein subunit beta-like prot	86.21%	1.23	6.23E-03	1.44	1.60E-04	1.15	0.04
P38013	AHP1	Peroxiredoxin type-2	37.50%	0.86	0.08	0.43	8.74E-03	0.86	0.17
P38144	ISW1	ISWI chromatin-remodeling complex ATPase ISW1	26.61%	NA	NA	NA	NA	0.09	0.44
P38236	MUM2	Protein MUM2	26.47%	NA	NA	2.26	0.05	NA	NA
P38701	RPS20	40S ribosomal protein S20	83.33%	1.00	0.99	1.04	0.62	1.12	0.12
P38707	DED81	Asparaginyl-tRNA synthetase, cytoplasmic	64.81%	1.40	0.02	1.01	0.87	0.97	0.71
P38708	YHR020W	Putative prolyl-tRNA synthetase YHR020W	60.42%	1.14	0.14	1.06	0.81	0.80	0.17
P38720	GND1	6-phosphogluconate dehydrogenase, decarboxylating 1	78.57%	1.03	0.55	0.87	0.02	0.98	0.69
P38746	YLF2	Putative GTP-binding protein YLF2	27.91%	1.11	0.17	1.48	0.09	NA	NA
P38754	RPL14B	60S ribosomal protein L14-B	63.64%	NA	NA	NA	NA	1.21	0.03
P38760	MIP6	RNA-binding protein MIP6	18.18%	NA	NA	NA	NA	1.54	0.39
P38788	SSZ1	Ribosome-associated complex subunit SSZ1	47.06%	NA	NA	0.82	4.31E-03	NA	NA
P38840	ARO9	Aromatic amino acid aminotransferase 2	34.04%	NA	NA	NA	NA	0.86	0.15
P38852	LIN1	Protein LIN1	21.43%	2.02	0.01	NA	NA	0.95	0.46
P38889	SKN7	Transcription factor SKN7	30.51%	NA	NA	NA	NA	1.15	0.81
P38910	HSP10	10 kDa heat shock protein, mitochondrial	45.45%	NA	NA	NA	NA	1.58	0.14
P38999	LYS9	Saccharopine dehydrogenase [NADP+, L-glutamate-formin	31.82%	0.36	1.91E-06	0.22	3.10E-07	0.87	8.92E-03
P39003	HXT6	High-affinity hexose transporter HXT6	65.85%	NA	NA	NA	NA	0.37	2.15E-05
P39077	CCT3	T-complex protein 1 subunit gamma	25.49%	0.31	0.07	0.01	0.02	1.10	0.86
P39516	RPS14B	40S ribosomal protein S14-B	57.14%	0.55	0.01	1.09	0.25	NA	NA
P39533	ACO2	Probable aconitase hydratase 2	37.31%	NA	NA	0.25	2.05E-03	NA	NA
P39708	GDH3	NADP-specific glutamate dehydrogenase 2	25.93%	1.31	0.76	4.64	0.12	0.78	0.05
P39741	RPL35A	60S ribosomal protein L35	84.62%	0.98	0.66	1.09	0.01	1.11	0.02
P39939	RPS26B	40S ribosomal protein S26-B	100.00%	1.15	0.03	1.18	0.03	1.21	0.02
P39954	SAH1	Adenosylhomocysteinase	63.41%	0.97	0.74	0.93	0.39	1.17	0.34
P39980	SIT1	Siderophore iron transporter 1	32.81%	NA	NA	NA	NA	0.48	0.72
P39997	NPP2	Ectonucleotide pyrophosphatase/phosphodiesterase 2	31.82%	NA	NA	NA	NA	1.25	0.40
P40010	NUG1	Nuclear GTP-binding protein NUG1	22.45%	NA	NA	0.90	0.51	NA	NA
P40016	RPN3	26S proteasome regulatory subunit RPN3	33.80%	0.88	0.06	NA	NA	1.02	0.75
P40017	YAT2	Carnitine O-acetyltransferase YAT2	32.93%	0.97	0.89	1.09	0.56	1.08	0.74
P40039	FCY21	Purine-cytosine permease FCY21	19.15%	0.96	0.69	0.95	0.49	0.85	0.23
P40069	KAP123	Importin subunit beta-4	38.10%	1.08	0.48	1.05	0.52	NA	NA

P40212	RPL13B	60S ribosomal protein L13-B	81.82%	0.96	0.11	1.01	0.78	0.98	0.47
P40213	RPS16A	40S ribosomal protein S16	63.64%	1.06	0.03	1.05	0.22	1.12	0.01
P40511	SPO22	Sporulation-specific protein 22	24.79%	0.03	0.25	NA	NA	2.62	0.47
P40559	INP51	Inositol-1,4,5-trisphosphate 5-phosphatase 1	14.29%	1.49	0.67	NA	NA	NA	NA
P40568	DSN1	Kinetochore-associated protein DSN1	24.07%	NA	NA	NA	NA	0.97	0.61
P41056	RPL33B	60S ribosomal protein L33-B	66.67%	NA	NA	NA	NA	1.04	0.61
P41277	RHR2	(DL)-glycerol-3-phosphatase 1	70.59%	1.42	2.97E-03	1.20	6.39E-03	1.15	0.13
P41807	VMA13	V-type proton ATPase subunit H	44.29%	0.91	0.49	1.00	0.97	1.03	0.77
P41940	PSA1	Mannose-1-phosphate guanylttransferase	61.76%	0.76	0.05	0.83	0.03	0.82	2.43E-03
P42942	YGR210C	Uncharacterized GTP-binding protein YGR210C	33.33%	1.25	0.14	0.68	8.28E-03	0.98	0.79
P43572	EPL1	Enhancer of polycomb-like protein 1	27.87%	1.38	0.63	NA	NA	NA	NA
P43638	MHP1	MAP-homologous protein 1	36.00%	1.05	0.76	NA	NA	NA	NA
P46655	GUS1	Glutamyl-tRNA synthetase, cytoplasmic	53.33%	1.01	0.85	1.37	3.81E-03	1.10	0.18
P46681	DLD2	D-lactate dehydrogenase [cytochrome] 2, mitochondrial	29.09%	NA	NA	NA	NA	1.04	0.57
P46990	RPL17B	60S ribosomal protein L17-B	90.00%	1.14	0.17	1.25	0.12	1.13	0.17
P47039	BNA3	Probable kynurenine--oxoglutarate transaminase BNA3	27.50%	0.61	2.12E-04	NA	NA	0.57	6.75E-03
P47061	VPS53	Vacuolar protein sorting-associated protein 53	23.85%	NA	NA	NA	NA	0.85	0.33
P47104	RAV1	Regulator of V-ATPase in vacuolar membrane protein 1	21.77%	NA	NA	NA	NA	0.11	0.43
P47141	RSM26	37S ribosomal protein S26, mitochondrial	23.33%	NA	NA	NA	NA	1.07	0.11
P47143	ADO1	Adenosine kinase	61.29%	0.66	5.76E-03	0.56	1.88E-05	1.04	0.71
P47161	VPS70	Vacuolar protein sorting-associated protein 70	22.97%	0.75	0.11	0.54	0.26	0.95	0.68
P48164	RPS7B	40S ribosomal protein S7-B	66.67%	NA	NA	NA	NA	0.99	0.90
P48563	MON2	Protein MON2	24.00%	NA	NA	0.89	0.45	NA	NA
P48570	LYS20	Homocitrate synthase, cytosolic isozyme	35.48%	0.93	0.32	0.25	1.23E-04	0.88	0.16
P48589	RPS12	40S ribosomal protein S12	73.33%	1.58	0.04	2.21	6.57E-06	1.37	0.13
P49090	ASN2	Asparagine synthetase [glutamine-hydrolyzing] 2	26.67%	2.18	0.21	NA	NA	NA	NA
P49167	RPL38	60S ribosomal protein L38	88.89%	NA	NA	1.60	4.78E-04	NA	NA
P49626	RPL4B	60S ribosomal protein L4-B	92.86%	0.98	0.70	1.27	3.46E-03	1.14	0.06
P49723	RNR4	Ribonucleoside-diphosphate reductase small chain 2	62.50%	NA	NA	0.78	0.03	NA	NA
P49956	CTF18	Chromosome transmission fidelity protein 18	25.68%	1.34	0.03	NA	NA	0.97	0.85
P53030	RPL1A	60S ribosomal protein L1	88.00%	1.00	0.95	1.01	0.68	1.16	0.04
P53067	KAP114	Importin subunit beta-5	30.00%	1.16	0.17	1.17	0.24	0.98	0.54
P53131	PRP43	Pre-mRNA-splicing factor ATP-dependent RNA helicase PRP43	24.68%	4.64	0.03	NA	NA	0.83	0.02
P53163	MNP1	54S ribosomal protein L12, mitochondrial	38.89%	NA	NA	NA	NA	1.10	0.42
P53202	CUL3	Cullin-3	22.62%	0.96	0.58	NA	NA	0.84	0.15
P53248	PEX8	Peroxisomal biogenesis factor 8	33.33%	NA	NA	NA	NA	0.36	0.51
P53912	YNL134C	Uncharacterized protein YNL134C	40.63%	1.28	0.08	NA	NA	NA	NA
P54115	ALD6	Magnesium-activated aldehyde dehydrogenase, cytosolic	50.00%	1.01	0.90	0.94	0.77	0.79	0.20
P54780	RPL15B	60S ribosomal protein L15-B	61.54%	NA	NA	1.09	0.22	NA	NA
Q00955	ACC1	Acetyl-CoA carboxylase	46.23%	1.19	0.53	1.01	0.97	1.35	0.17
Q01855	RPS15	40S ribosomal protein S15	100.00%	1.01	0.91	0.87	0.14	1.02	0.82
Q02685	RMI1	RecQ-mediated genome instability protein 1	33.33%	NA	NA	NA	NA	1.25	0.60
Q02884	ELP4	Elongator complex protein 4	22.73%	NA	NA	0.54	0.29	NA	NA
Q03161	YMR099C	Glucose-6-phosphate 1-epimerase	61.29%	0.80	1.56E-03	0.82	2.79E-04	0.92	0.24
Q03281	HEH2	Inner nuclear membrane protein HEH2	19.30%	0.79	9.57E-03	NA	NA	NA	NA
Q03530	RCE1	CAAX prenyl protease 2	11.32%	NA	NA	NA	NA	3.02	7.56E-03
Q03631	WAR1	Weak acid resistance protein 1	18.60%	1.59	0.09	1.33	0.40	0.68	0.09

Q03758	BUL2	Ubiquitin ligase-binding protein BUL2	28.57%	NA	NA	NA	NA	0.45	0.07
Q04120	TSA2	Peroxiredoxin TSA2	33.33%	0.99	0.88	0.92	0.14	1.13	0.14
Q04601	APC4	Anaphase-promoting complex subunit 4	18.06%	0.72	0.18	0.82	0.34	0.75	0.06
Q04693	RSE1	Pre-mRNA-splicing factor RSE1	23.13%	0.86	0.01	0.87	0.09	1.02	0.78
Q05029	BCH1	Protein BCH1	23.46%	1.07	0.81	0.90	0.67	1.27	0.45
Q05498	FCF1	rRNA-processing protein FCF1	31.58%	0.35	0.06	NA	NA	NA	NA
Q05549	HRQ1	Putative ATP-dependent helicase HRQ1	18.82%	NA	NA	NA	NA	0.41	0.36
Q06178	NMA1	Nicotinamide-nucleotide adenylyltransferase 1	38.24%	NA	NA	1.08	0.18	NA	NA
Q06408	ARO10	Transaminated amino acid decarboxylase	28.57%	NA	NA	NA	NA	1.19	0.04
Q07478	SUB2	ATP-dependent RNA helicase SUB2	41.03%	1.01	0.96	1.32	0.05	1.18	0.04
Q07527	TRM3	tRNA guanosine-2'-O-methyltransferase TRM3	22.92%	0.73	1.67E-03	NA	NA	1.02	0.88
Q07799	YLL007C	Uncharacterized protein YLL007C	24.00%	NA	NA	NA	NA	2.04	0.31
Q07878	VPS13	Vacuolar protein sorting-associated protein 13	27.47%	NA	NA	NA	NA	7.01	0.55
Q08230	EMIS	Succinate dehydrogenase assembly factor 2, mitochondria	55.00%	NA	NA	0.46	0.62	NA	NA
Q08438	VHS3	Phosphopantothenoylcysteine decarboxylase subunit VHS3	22.50%	0.97	0.65	0.58	0.05	0.87	0.65
Q08562	ULS1	ATP-dependent helicase ULS1	25.32%	NA	NA	0.84	0.50	NA	NA
Q08754	BUD7	Bud site selection protein 7	25.30%	NA	NA	NA	NA	0.73	0.26
Q08972	NEW1	[NU+] prion formation protein 1	36.15%	NA	NA	NA	NA	1.08	0.60
Q12031	ICL2	Mitochondrial 2-methylisocitrate lyase	28.00%	0.80	0.04	0.82	0.18	0.84	0.04
Q12080	NOP53	Ribosome biogenesis protein NOP53	29.73%	NA	NA	0.88	0.51	NA	NA
Q12150	CSF1	Protein CSF1	17.29%	NA	NA	0.05	0.17	NA	NA
Q12167	RRG1	Required for respiratory growth protein 1, mitochondrial	29.17%	NA	NA	NA	NA	1.74	0.29
Q12213	RPL7B	60S ribosomal protein L7-B	85.00%	1.29	7.00E-04	1.27	0.02	0.87	0.46
Q12250	RPN5	26S proteasome regulatory subunit RPN5	34.43%	0.19	0.18	NA	NA	2.73	0.46
Q12325	SUL2	Sulfate permease 2	29.11%	NA	NA	0.60	0.35	NA	NA
Q12341	HAT1	Histone acetyltransferase type B catalytic subunit	18.92%	NA	NA	NA	NA	0.77	0.07
Q12447	PAA1	Polyamine N-acetyltransferase 1	26.32%	1.04	0.66	1.05	0.56	0.92	0.39
Q12460	NOP56	Nucleolar protein 56	26.42%	1.40	6.82E-03	1.41	0.02	0.95	0.56
Q12749	SMC6	Structural maintenance of chromosomes protein 6	26.26%	0.98	0.80	0.61	0.30	NA	NA
Q3E757	RPL11B	60S ribosomal protein L11-B	63.64%	1.02	0.55	1.31	4.39E-03	1.17	0.01
Q3E835	YOL086W-A	Uncharacterized protein YOL086W-A	28.57%	1.01	0.96	NA	NA	NA	NA
Q92392	YOL103W-A	Transposon Ty1-OL Gag polyprotein	12.50%	0.85	0.03	1.11	0.31	0.96	0.46